STRUCTURE AND ACTIVITY OF

PSEUDOMONAS AERUGINOSA PAO1 BIOFILMS

by

Raaja Raajan Angathevar Veluchamy

A thesis submitted in partial fulfillment
of the requirements for the degree

of

Master of Science

in

Environmental Engineering

MONTANA STATE UNIVERSITY
Bozeman, Montana

April 2006

APPROVAL

of a thesis submitted by

Raaja Raajan Angathevar Veluchamy

This thesis has been read by each member of the thesis committee and has been found to be satisfactory regarding content, English usage, format, citations, bibliographic style, and consistency, and is ready for submission to the Department of Graduate Education.

Dr. Zbigniew Lewandowski

Approved for the Department of Chemical and Biological Engineering

Dr. Ron Larsen

Approved for the Department of Graduate Education

Dr. Joseph J. Fedock

STATEMENT OF PERMISSION TO USE

In presenting this thesis in partial fulfillment of the requirements for a master's degree at Montana State University, I agree that the Library shall make it available to borrowers under rules of the Library.

If I have indicated my intention to copyright this thesis by including a copyright notice page, copying is allowable only for scholarly purposes, consistent with "fair use" as prescribed in the U.S. Copyright Law. Requests for permission for extended quotation from or reproduction of this thesis in whole or in parts may be granted only by the copyright holder.

Raaja Raajan Angathevar Veluchamy

April 2006

TABLE OF CONTENTS

TABLE OF CONTENTS - CONTINUED

LIST OF TABLES

LIST OF FIGURES

Figure Page

Figure Page

Figure Page

Figure Page

NOMENCLATURE

A	m^2	surface area of the electrode
AP		areal porosity
AP_{CV}	%	coefficient of variation of areal porosity in a given biofilm layer image
AP_{SD}		standard deviation of areal porosity in a given biofilm layer image
b	1/s	Decay coefficient
C	Kg/m^3	limiting nutrient concentration
C_0	$moles/m^3$	bulk ferricyanide concentration
C_1, C_2, …	Kg/m^3	nutrient concentrations in multi-nutrient biofilms
C_b	Kg/m^3	limiting nutrient concentration in the bulk
C_{CV}	%	coefficient of variation of surface averaged local dissolved oxygen concentration
C_L	Kg/m^3	local dissolved oxygen concentration
C_{min}	Kg/m^3	minimum nutrient concentration at which microorganism can grow in biofilm
C_s	$moles/m^3$	ferric cyanide concentration at the tip of the microelectrode
C_{SA}	Kg/m^3 (unless specified)	surface averaged dissolved oxygen concentration
C_{SD}	Kg/m^3 (unless specified)	standard deviation of surface averaged local dissolved oxygen concentration

D_{CN}	m^2/s	diffusivity of ferricyanide
D_{CV}	%	coefficient of variation of surface averaged local relative effective diffusivity
D_f	m^2/s	effective diffusivity
D_{fz}	m^2/s	surface averaged effective diffusivity
D_L	-	local relative effective diffusivity
D_m	m^2/s	diffusivity of oxygen in the membrane
D_r		relative effective diffusivity in biofilm
D_{SA}	-	surface averaged relative effective diffusivity
D_{SD}		standard deviation of surface averaged relative effective diffusivity
D_W	m^2/s	diffusion in liquid phase
F	coulomb	faraday constant
f_d		fraction of the microorganism in a multispecies biofilm
I	ampere	electric current
i		location in the biofilm where the microelectrode measurements were done
J	$Kg/m^2/s$	flux of a nutrient to the biofilm surface
J_f	$moles/m^2/s$	flux of ferric cyanide to the electrode surface
k	1/s	minimum utilization rate
k_0	m/s	composite overall mass transfer coefficient including the resistances in both the phases
k_f	m/s	mass transfer coefficient
K_s	Kg/m^3	half-saturation constant

K_{S1}, K_{S2}, …	Kg/m^3	half-saturation constant of each species in the multispecies biofilm
L_f	m	average biofilm thickness
n		number of moles of electrons
C_{02}	mg/L	dissolved oxygen concentration
P_d		probability of division
Pe		probability of erosion
q		index number of segments of each layered image
t	s	Time
X	Kg/m^3	cell density
X_f	Kg/m^3	Biofilm density
$Y_{x/c}$		yield coefficient (kg microorganism grown/kg nutrient consumed)
Z_m	m	membrane thickness
z	m (unless specified)	distance from the bottom of the biofilm
ζ	$m^2/s/m$	Effective diffusivity gradient
δ	m	mass transfer boundary layer thickness near microelectrode tip
μ	1/s	specific growth rate
κ		Monod-like constant used in cellular automata models
τ		shear stress

σ		Biofilm strength (cohesion)
μ_{max}	1/s	maximum specific growth rate
Δz	m	distance between two adjacent layers in the biofilm

ABSTRACT

Nutrient concentration profiles are affected by the mass transport outside the biofilm, inside the biofilm, and by the structure of the biofilm. To understand the distribution of biofilm activity, it is necessary to correlate the local nutrient concentration, local mass transport in the biofilm and the biofilm structure. The correlations among surface averaged dissolved oxygen concentration, surface averaged relative effective diffusivity, and areal porosity in the biofilms of *Pseudomonas aeruginosa PAO1* grown in a flat plate reactor, were quantified. Three dimensional distributions of local dissolved oxygen concentration, local relative effective diffusivity, and porosity in the biofilm were measured. It was found that the local dissolved oxygen concentrations and relative effective diffusivities correlate weakly with each other or with the areal porosity. However surface averaged dissolved oxygen concentration and surface averaged relative effective diffusivity strongly correlated with each other and with the areal porosity. The surface averaged dissolved oxygen concentration, surface averaged relative effective diffusivity, and areal porosity decreased towards the bottom of the biofilm, while the coefficients of variation computed for each of these parameters increased towards the bottom of the biofilm. The coefficient of variation is quantified as a measure of the heterogeneity of the biofilm. The increase in the coefficient of variation shows that the heterogeneity of the biofilm increases towards the bottom of the biofilm.

INTRODUCTION

Project Background

The W.M. KECK Foundation awarded the Center for Biofilm Engineering (CBE), Montana State University (MSU) $1,000,000 to support a multidisciplinary research program for investigating microbial biofilm formation as a developmental process. The purpose of the project was to create an innovative research team that will allow the investigation of the multicellular nature of life in a bacterial biofilm in a comprehensive and integrated way. CBE took an engineering systems approach to this problem because the bacteria in a biofilm interact in complex physical, chemical, and biological ways. The key to understanding the multicellular developmental process of biofilm formation is integrating the information collected in one experimental system. The overall technical objective of this project was to integrate quantitative spatial and temporal measurements of genetic, physiological, chemical, and mechanical parameters measured in a single biofilm system. The research team selected *Pseudomonas aeruginosa* PAO1 as the model biofilm because of its importance in medical science.

The Biofilm Structure and Function group (CBE, MSU) is one of the research team members which participated in the research program sponsored by the W.M. KECK Foundation. This group is well known for microscale biofilm research and has the experimental capabilities to measure local nutrient

concentrations and local mass transport parameters using microelectrodes in addition to the capability of quantifying three-dimensional biofilm structure. The Structure and Function group set itself a goal of studying the chemical and structural heterogeneity of *Pseudomonas aeruginosa* PAO1 biofilms using state-of-the-art microelectrodes and confocal microscopy. This thesis partly fulfills the goal of the Structure and Function group in studying the chemical and structural heterogeneity of *Pseudomonas aeruginosa* PAO1 biofilms.

There are many ways to characterize biofilms, and one of them is to quantify the relation between the structure of the biofilm and its activity. Many parameters affect the structure and activity of the biofilm; we have selected only those which, in our opinion, are the most relevant: distribution of the biomass, distribution of the dissolved oxygen concentration and distribution of the relative effective diffusivity. Quantification of these parameters will provide an understanding of the microbial processes in the biofilm. In addition, experimental verification of the relations among these three parameters can be used to verify and modify mathematical models of biofilms.

Goal

The goal of this thesis is to characterize *Pseudomonas aeruginosa* PAO1 biofilms using the conceptual model of stratified biofilms. In the framework of this model the distribution of the following surface averaged parameters will be

correlated: effective diffusivity (and the equivalent distribution of biomass density), areal porosity, and dissolved oxygen concentration.

Research Strategy

The challenge in achieving the thesis goal is to quantify the following parameters at the same location in the biofilm: 3-D distribution of the relative effective diffusivity, 3-D distribution of the dissolved oxygen concentration and 3-D distribution of areal porosity.

Within the Structure and Function research group, we have mastered the techniques needed to quantify the distributions of effective diffusivity, biomass density, oxygen concentration and porosity in biofilms. We will attempt to describe the relations among these parameters using the conceptual model of stratified biofilms, which compares average values of the parameters measured over a specified surface area and at specified distances from the bottom of the biofilm. The working hypothesis of this research is equivalent to the main assumption of the conceptual model of stratified biofilms, that the measured parameters within the space occupied by the biofilm are related when quantified as average values in layers of the biofilm, but that these relations are not necessarily obvious when analyzing individual measurements. We will verify this hypothesis.

The measurement of local dissolved oxygen concentration and the acquisition of confocal laser scanning microscopy images are nondestructive

processes (i.e., the biofilm is active after the procedure), while the measurement of the relative effective diffusivity in a biofilm is a destructive process (i.e., the biofilm is not metabolically active during the procedure). Thus, the dissolved oxygen concentration was measured first, followed by confocal laser scanning microscopy imaging of the biofilm structure; the relative effective diffusivity in the biofilm was measured last. The biofilm is conceptually subdivided into several layers at different distances from the bottom of the biofilm. For each such layer, three parameters (relative effective diffusivity, dissolved oxygen concentration, and areal porosity) are measured at several locations. To characterize the relations among the measured parameters in the biofilm, the pairs of these parameters were correlated with each other:

1. areal porosity and dissolved oxygen concentration.
2. areal porosity and relative effective diffusivity.
3. dissolved oxygen concentration and relative effective diffusivity.

The results of this work characterize the structure and activity of Pseudomonas *aeruginosa* PAO1 biofilms, which are the object of study of the project sponsored by the W.M. KECK Foundation. However, the practical applications of these results extend beyond the scope of this study. The correlation between dissolved oxygen concentration and areal porosity can be used to verify the predictions of the mathematical models based on cellular automata. The correlation between the relative effective diffusivity and the

dissolved oxygen concentration can be used to verify the predictions based on the mathematical model of stratified biofilms.

Tasks

To accomplish the thesis goal, the following tasks were planned:

1. Grow *Pseudomonas aeruginosa* PAO1 biofilms in flat plate biofilm reactors.
2. Quantify:
    - 3-D distribution of dissolved oxygen concentration.
    - 3-D distribution of areal porosity.
    - 3-D distribution of local relative effective diffusivity.
3. Correlate:
    - Local dissolved oxygen concentration and local relative effective diffusivity.
    - Local dissolved oxygen concentration and areal porosity.
    - Local relative effective diffusivity and areal porosity.
4. Quantify variation of the following parameters in each layer of the biofilm:
    - Local dissolved oxygen concentration.
    - Areal porosity.
    - Local relative effective diffusivity.

Biofilm Structure and Activity

Biofilm Structure.

This project requires the quantification of biofilm structure. Biofilm structure is defined as the distribution of biomass in a biofilm. It is well known that biofilm structure affects mass transfer and activity in biofilms (Beyenal and Lewandowski, 2005b; Yang and Lewandowski, 1995; Picioreanu et al., 2000b; Noguera et al., 1999). Biofilms are composed of dense cell clusters separated by crevasses or water channels of various sizes through which solute and suspended particles can migrate (Rasmussen and Lewandowski, 1998; Stoodley et al., 1997; deBeer et al., 1996; deBeer et al., 1994a; deBeer et al., 1994b; Beyenal et al., 2004b). The nutrients for biofilm growth are transferred via diffusion and convection from bulk to biofilm surface, and then to the inner portion of the biofilm, where they are consumed by microorganisms. The biofilm structure is quantified by its density, porosity, thickness, pore structure, pore/channel pattern, and diffusion distance, all of which influence the mass transfer rate and biofilm activity (Bishop ,1997; Yang and Lewandowski, 1995; deBeer et al., 1997; Beyenal et al., 1998). Mass transfer from the bulk solution to the biofilm is mainly controlled by the bulk nutrient concentration and the flow velocity at which the biofilm is grown. Meanwhile, the nutrient consumption rate in the biofilm is controlled by the density of the microorganisms and the concentration of the growth-limiting nutrient. It is well known that the structure

and activity of the biofilm influence each other. A porous structure helps transport the nutrients to the deeper layers of the biofilm and increases the nutrient concentration in the space occupied by the biofilm.

There are many tools available to analyze biofilm structure, from simple light microscopy to sophisticated confocal laser scanning microscopy (CLSM). The digitized images of biofilms are used to quantify biofilm structure (Beyenal et al., 2004b; Beyenal et al., 2004a). Porosity is a well-known parameter describing biofilm structure. There are two different descriptions of porosity: 1) areal and 2) volumetric. Areal porosity is the ratio of the total void surface area to the total surface area of a biofilm. Volumetric porosity is the ratio of the total void volume to the total biofilm volume; this is calculated from CLSM images.

The knowledge of biofilm structure alone provides very little information unless it is correlated with the local nutrient concentration or the local effective diffusivity. Local nutrient concentrations are used to generate a concentration profile and to calculate the activity of the biofilm, i.e. the flux of nutrients to the biofilm. The local effective diffusivity reflects the mass transport property of the biofilm and is related to the density of the biofilm according to the Eqn. 1.1 (Fan et al., 1990):

$$D_r = 1 - \frac{0.43 X_f^{0.92}}{11.19 + 0.27 X_f^{0.99}} \qquad \text{Eqn. 1.1}$$

Biofilm Activity

Biofilm activity is defined as the flux of the growth-limiting nutrient to the surface of the biofilm. The activity of a microorganism is defined as the substrate consumption rate per unit volume of suspension. The activity of the microorganisms in the biofilm is often estimated to be the same as the activity of microorganisms in suspended cultures. The nutrient consumption rate is calculated from the specific growth rate, which is described by the well-known Monod equation (Eqn. 1.2). The nutrient utilization rate is given by Eqn. 1.3. The flux of a nutrient to the biofilm surface (J) is calculated as calculated according to Eqn. 1.4. dC/dz @ z = L_f is calculated from the experimentally measured profile (i.e. the dissolved oxygen profile).

$$\mu = \mu_{max} \frac{C}{K_s + C}$$

Eqn. 1.2

$$-\frac{dC}{dt} = \frac{\mu.X}{Y_{X/C}}$$

Eqn. 1.3

$$J = D_w \left.\frac{dC}{dz}\right|_{z=L_f}$$

Eqn. 1.4

Conceptual Models of Biofilm Structure

The description of biofilm processes to some extent depends on the conceptual model of biofilm structure. Some phenomena that exist in heterogeneous biofilms do not exist in homogenous biofilms, such as convective mass transport in the space occupied by the biofilm. The historical development of conceptual models of biofilm structure is depicted in Fig. 1.1.

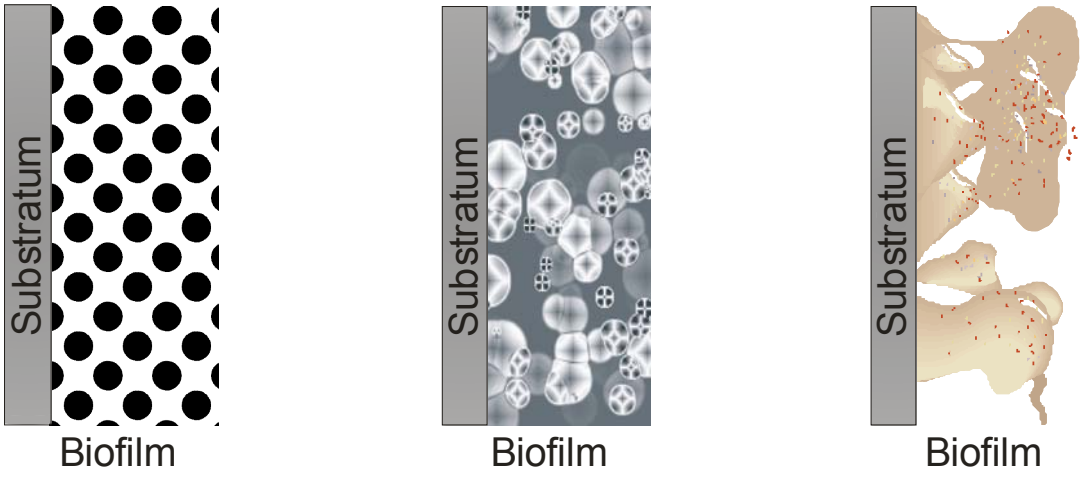

Fig. 1.1. Conceptual models of biofilms. (A) Homogenous biofilm, i.e. uniform matrix of extracellular polymers with homogenously distributed biomass; (B) multinutrient and multispecies biofilm; and (C) heterogeneous biofilm composed of nonuniformly distributed biomass concentrated in microcolonies separated by voids.

Mathematical Models of Biofilm Activity and Deposition

The development of the mathematical models of biofilms follows the development of the conceptual models of biofilm structure because biofilm structure defines the mechanisms of mass transport in the space occupied by the biofilm.

Mathematical Model of Homogenous Biofilms

Earlier biofilm models were derived from the models used in chemical engineering to describe diffusion-reaction in a porous catalyst particle (Williamson and McCarty, 1976; Atkinson and Davies, 1974). Biofilm was considered to be a uniform matrix with homogenously distributed biomass (Fig. 1.1A). The goal of these models was to predict the activity (nutrient flux) and the growth-limiting nutrient concentration profile of the biofilm.

In these models, the authors assumed that the nutrients were transferred via diffusion in the biofilm and that the rate of nutrient consumption was limited by a single nutrient, which was described by Monod growth kinetics. The thickness and density of the biofilm were assumed to be uniform in the biofilm. With these assumptions, the nutrient continuity equation for a steady state in the homogenous biofilm was given as:

$$\frac{d^2C}{dz^2} = \frac{kCX_f}{D_f(C + K_S)}$$

Eqn. 1.5

Since the nutrient continuity equation is a second-order differential equation, two boundary conditions are required for the solution:

@ z = 0 (bottom) dC/dz = 0

@ z = L_f (top) C = C_b

Since an inert surface is used to grow the biofilms, there will be no flux of nutrients at the bottom, so at the bottom dC/dz will be zero. At the surface of the biofilm (z = L_f), the nutrient concentration is C_b. It can either be calculated from the external mass transport coefficient or assumed to be equal to the bulk nutrient concentration. The general mass transfer relation is given by Eqn. 1.6.

$$J\big|_z = k_0(C - C_b)$$

Eqn. 1.6

Where k_0 can be a composite overall mass transfer coefficient which includes the resistance in both the phases. When there is no mass transfer resistance ($1/K_0$)→ 0 or K_0→ ∞ and hence from Eqn. 1.6 we get C=C_b @ z = L_f. When the mass transfer resistance is infinite ($1/K_0$)→ ∞ or K_0→ 0 and hence from from Eqn. 1.6 we get the no flux condition $J\big|_{z=0} = 0$

To solve Eqn. 1.5 it is necessary to know the biokinetic parameters (k, K_s), biofilm density (X_f), biofilm thickness (L_f), and effective diffusivity in the biofilm (D_f). These parameters must be input into the model; usually they are either measured or estimated from similarly operated reactors. For homogenous biofilms D_f is generally assumed to be 80% of the diffusivity of the nutrient in water (Wanner and Reichert, 1996b; Wanner and Reichert, 1996a; Wanner et al.,

1995; Wanner and Gujer, 1986; Morgenroth et al., 2000). Generally, the biokinetic parameters calculated for suspended culture are used for biofilm-type growth.

Eqn. 1.5 is a nonlinear equation which can not be solved analytically, so a numerical method is preferred. A mathematical model of a homogenous biofilm is shown schematically in Fig. 1.2. This model predicts the nutrient concentration profile and nutrient consumption rate in the biofilm.

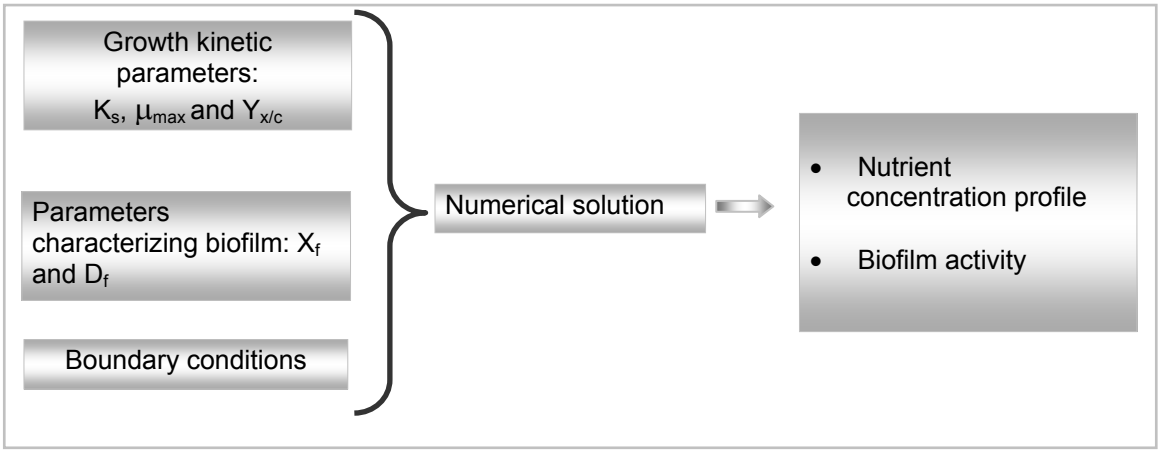

Fig. 1.2. Schematic description of earlier mathematical biofilm model developed by Williamson and McCarty (1976).

For unsteady state conditions, Eqn. 1.5 can be written as

$$\frac{\partial C}{\partial t} = D_f \frac{\partial^2 C}{\partial z^2} - \frac{kCX_f}{(C + K_S)}$$

Eqn. 1.7

Rittmann et al. improved the homogenous biofilm model by solving Eqn. 1.7 numerically and algebraically (using approximations) to predict the flux of the growth-limiting nutrient to the biofilm for unsteady state conditions (Rittmann and McCarty, 1980a; Rittmann and McCarty, 1980b). In addition, they introduced the

minimum nutrient concentration (C_{min}) at which microorganisms can grow in the biofilm. Below this concentration, there is no microbial activity. C_{min} is calculated from the following equation:

$$C_{min} = \frac{K_s b}{Y_{x/c} k - b}$$

Eqn. 1.8

Mathematical Model of Multispecies and Multinutrient Biofilms

The nest step in the development of the homogenous biofilm model was the inclusion of multiple species of microorganisms and the delivery of different nutrients to different physiological groups of microorganisms. Rittmann and Dovantzis (1983) developed a biofilm model which could accommodate multiple nutrients and multiple species in the biofilms.

The multispecies, multinutrient biofilm model was an improvement of the model developed by Rittmann and McCarty (1980a,b). The growth rate of microorganisms is described by multiple Monod equations in this model:

$$\mu = \mu_{max} \left(\frac{C_1}{K_{s1} + C_1} \right) \left(\frac{C_2}{K_{s2} + C_2} \right)$$

Eqn. 1. 9

To determine the nutrient growth limitation, the nutrient continuity equation for the biofilm must include all the nutrients and it must be solved for all of them simultaneously. The model predicts the flux of nutrients to the biofilm and the growth-limiting nutrient in the biofilm. The model also quantifies the space occupied by each species of microorganism in the biofilm (Fig. 1.3). The model

incorporates simultaneous nutrient utilization and diffusion within the biofilm, and external mass-transport resistance from the bulk liquid to the biofilm surface. The growth of the biomass is proportional to the nutrient utilization rate, the biomass loss from endogenous respiration, and the detachment and formation of inert biomass.

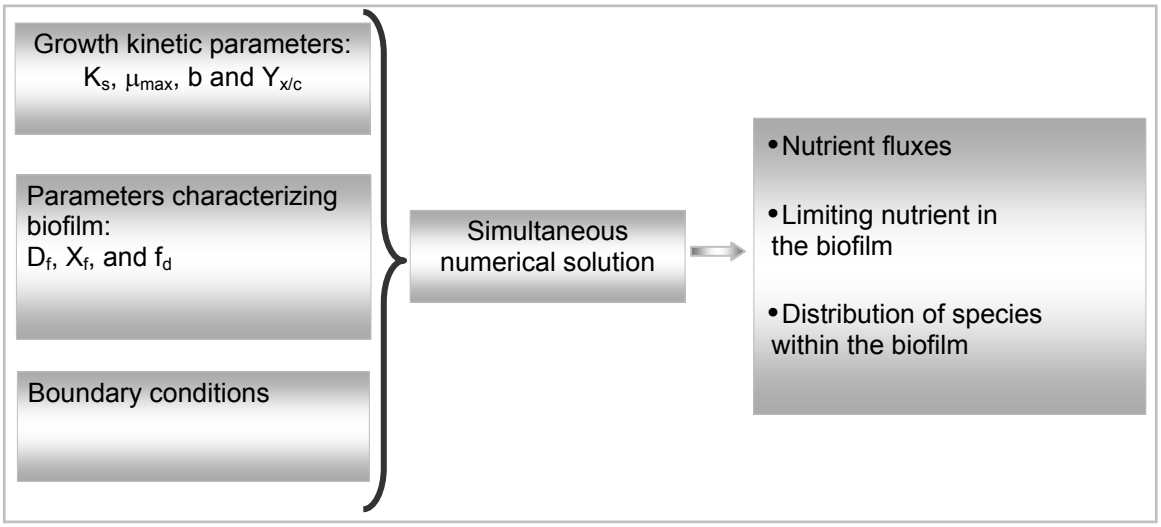

Fig. 1.3. Schematic representation of the mathematical model of multispecies, multinutrient biofilms.

These models were applied with small modifications to many biofilm processes (Williamson and McCarty, 1976; Suidan et al., 1994; Sun et al., 1998; Soda et al., 1999; Stewart et al., 1996). One of these models was “Biosim” (Wanner and Gujer, 1986), which was improved later to include irregular biofilm structure and renamed as “Aquasim” (Wanner and Reichert, 1996a; Wanner et al., 1995; Wanner and Reichert, 1996b). Aquasim was an advanced version of the model that included diffusive transport of particulate components in the

biofilm matrix, changes in biofilm porosity, changes in effective diffusivity, and simultaneous attachment/detachment of cells and particles at the biofilm surface. Aquasim allowed users to select the input operational parameters in biofilm processes, and it predicted the nutrient flux, microbial volume fraction, and nutrient concentration profile.

Mathematical Models of Biofilms Based On Cellular Automata

With the arrival of the conceptual model of heterogeneous biofilms (Fig. 1.1C) the models of biofilm activity and accumulation needed to include the structure of the biofilm. One such attempt used cellular automata to imitate biofilm structure (Wimpenny et al., 2000). The cellular automata (CA) model was developed from the “Game of Life”. The “Game of Life” consisted of simple rules such as: cells live, divide or die according to the occupancy of the spaces adjacent to them (Wimpenny et al., 2000).

CA is a discrete dynamic model often described as a counterpart to models based on differential equations. The term discrete refers to the space, time and properties of the system. They are described as dynamic because they evolve over time. Colasanti applied CA principles to biofilm modeling for the first time in 1992. Later the same author developed an improved CA model (Wimpenny and Colasanti, 1997a; Wimpenny and Colasanti, 1997b).

The simple biofilm model based on CA was refined by Picioreanu et al. (1998a,b), who used a much more realistic model. Their efforts were then

followed by those of others (Kreft et al., 2001; Noguera et al., 1999; Picioreanu et al., 2001; Picioreanu et al., 2000b; Picioreanu et al., 2000a; Picioreanu et al., 1998b; Picioreanu et al., 1998a).

Since biofilm models based on CA were complex, Hermanowicz (2001) proposed a cellular automata model describing only the simplest case of a single-species biofilm with a single growth-limiting nutrient (Hermanowicz, 2001). Since most of the CA models focused on predicting biofilm structure rather than activity, Pizarro et al. (2001) developed a quantitative CA biofilm model capable of simulating heterogeneous structures while predicting nutrient concentration gradients, fluxes and steady-state biofilm conditions. They found that the predictions fit well to the predictions from the solution of one-dimensional differential equations (Pizarro et al., 2001). They concluded that CA models do not have a significant advantage over finite difference models when simulating homogenous biofilms. Similarly, Picioreanu et al. (2000) concluded that the two-dimensional model of the biofilm predicted similar biofilm activity to that predicted from a simple diffusion-reaction model (Picioreanu et al., 2000b).

Further improvement of the heterogeneous biofilm models came from Kreft et al. (2001), who developed an individual-based multinutrient, multispecies two-dimensional model of nitrifying biofilms to predict biofilm structures, i.e., surface enlargement, roughness, and diffusion distances. They compared the predicted structures with the predictions of the CA model (biomass-based model) developed by Picioreanu et al.(Picioreanu et al., 1998b; Picioreanu et al., 1998a)

and concluded that the two models delivered solutions that agreed in principle, but that they differed in details of biofilm shape and growth of minority species.

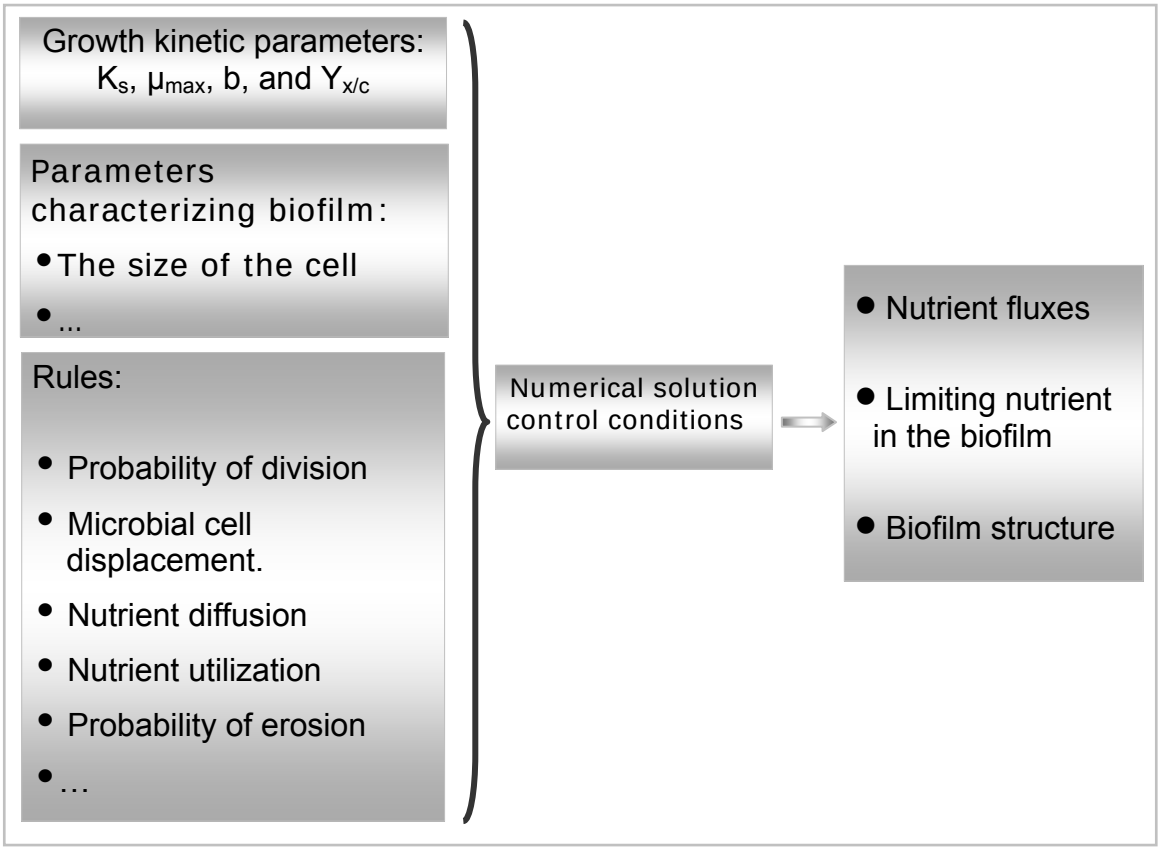

Fig. 1.4. Conceptual description of CA biofilm model.

In spite of extensive effort to model heterogeneous biofilms (Fig. 1.1C), the model predictions cannot be verified experimentally, while the CA-based models are able to replicate some of the experimental results albeit rather crudely (Wimpenny et al., 2000). There is no direct link between the CA model parameters and parameters such as effective diffusivities or reaction rate constants (Picioreanu et al., 2000b). Fig. 1.4 schematically represents the mathematical model based on CA (Hunt, S.M. et al., 2003).

Although the models based on cellular automata account for the heterogeneity of the biofilm, verification of the model results and associated rules is quite difficult. There is an ongoing effort to generate mathematical models of heterogeneous biofilms that can be verified experimentally. To overcome the limitations of the models based on cellular automata, Beyenal and Lewandowski, 2005a, introduced the concept of stratified biofilms.

Models of Stratified Biofilms

The model of stratified biofilms conceptually divides the biofilm into layers in an attempt to integrate experimental measurements with mathematical modelling. For example, in the stratified biofilm (Fig. 1.5), the dissolved oxygen concentration is measured over a surface for a given distance from the bottom. From these measurements, the average value of dissolved oxygen concentration is calculated to show the surface averaged dissolved oxygen concentration for that distance from the bottom. The same procedure is repeated for different layers separated by a distance of Δz in the biofilm. Typically, the value of Δz is approximately equal to the tip diameter of the microelectrode, or it may be thicker. Fig. 1.6 shows the surface averaged effective diffusivity profile of a heterogeneous biofilm (Beyenal and Lewandowski, 2002). The linear decrease in the relative effective diffusivity is due to the increasing biomass density towards the bottom of the biofilm (Eqn. 2.12). Even though Eqn. 2.12 gives a non-linear relation between the diffusivity and density of the biofilm, over a small range of density the diffusivity variation can be approximated as linear which provides the

physical mechanism behind the linear variation of the diffusivity towards the bottom of the biofilm. Fig. 1.7. shows the input and output parameters used in the model of stratified biofilms.

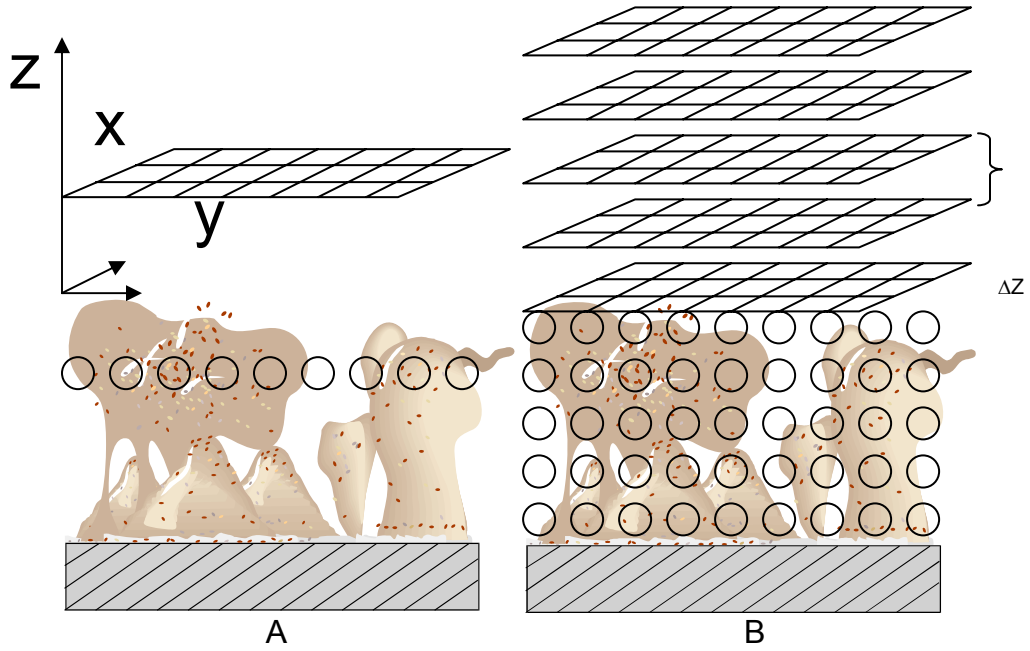

Fig. 1.5. Conceptual image of stratified biofilms. The space occupied by the biofilm is divided into layers and the parameters characterizing the biofilm are measured for each layer (A). The parameters are then averaged for each layer (B).

The nutrient continuity equation of the mathematical model of the stratified biofilm is given in Eqn. 1.10 (Beyenal and Lewandowski, 2005). The heterogeneity of the biofilm is introduced in the model equation (Eqn. 1.10) in the form of the relative effective diffusivity gradient (ζ). The parameter ζ has the same units as that of the mass transfer coefficient. Eqn. 1.10 is used to calculate the nutrient concentration in the stratified biofilm.

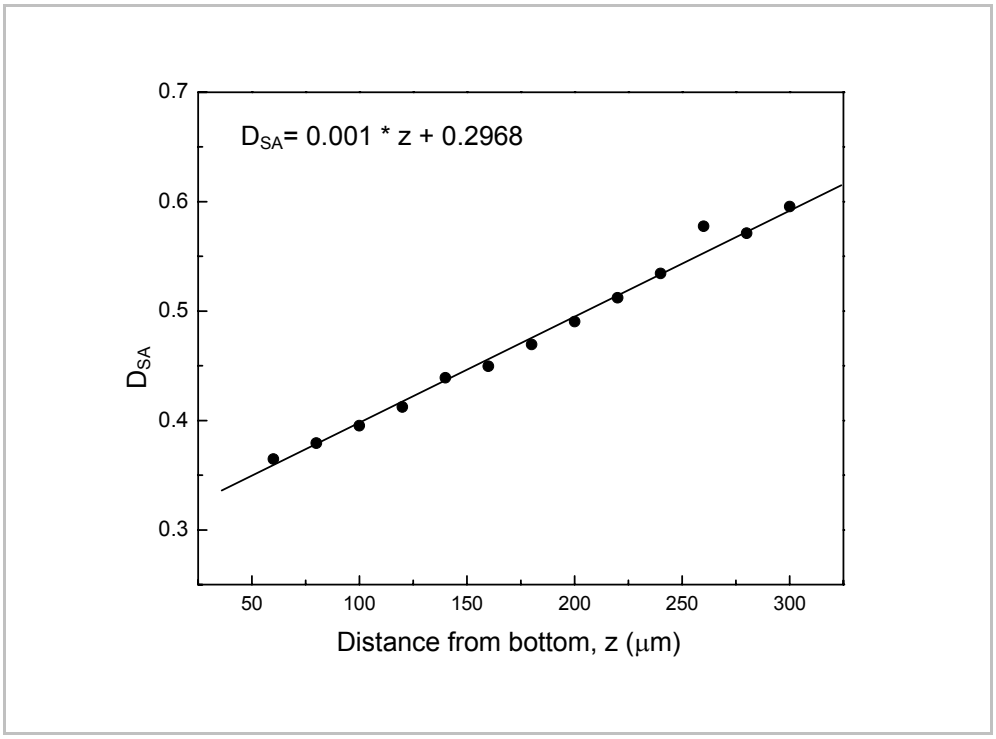

Fig. 1.6. An example of a relative surface averaged effective diffusivity profile reproduced from (Beyenal and Lewandowski, 2002).

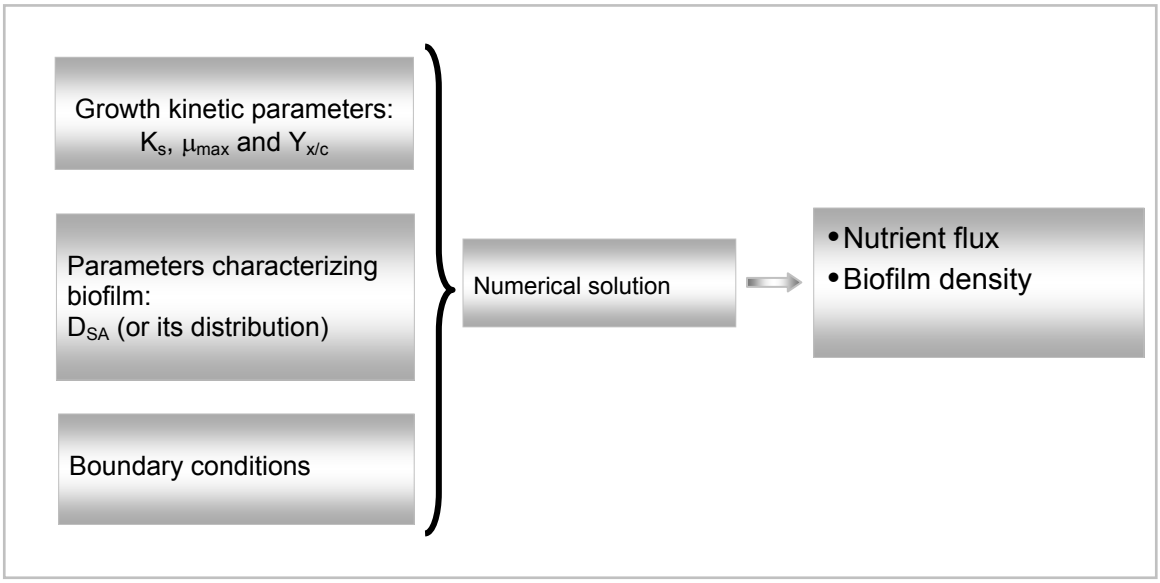

Fig. 1.7. Schematic representation of the mathematical model based on the stratified biofilm concept (Beyenal and Lewandowski, 2005).

$$D_{fz}\frac{d^2C_{SA}}{dz^2}+\zeta\frac{dC_{SA}}{dz}=\frac{\mu_{max}C_{SA}X_f}{Y_{x/c}(K_s+C_{SA})}$$

Eqn. 1.10

Verification of Mathematical Models

The data from this work can be used to verify the predictions of mathematical biofilm models based on the CA and stratified biofilm concepts. The mathematical biofilm models based on cellular automata (CA) have the unique feature of predicting the biofilm structure and the nutrient concentration distribution inside the predicted biofilm structure. The input parameters of the mathematical models based on CA can be adjusted so that the structures generated by these models are similar to the visual structures of natural biofilms. Even though the formations generated by models based on CA are visually similar to natural biofilms, it is not known whether the quantitative parameters (areal porosity and local nutrient concentration) calculated from these models reflect those measured in natural biofilms. The important pieces of information required to verify mathematical models based on CA are the three-dimensional distribution of the nutrient and the structure of natural biofilm. This work generates this information by quantifying the three-dimensional distribution of dissolved oxygen concentration at a selected location inside the biofilm and superimposing this information on the biofilm structure evaluated from CLSM images obtained at the same location.

Beyenal and Lewandowski (2005) demonstrated that the relative effective diffusivity varied linearly inside the three-species biofilm of *Pseudomonas aeruginosa*, *Pseudomonas fluorescens* and *Klebsiella pneumoniae.* Since this was done only once, this work generated profiles of effective diffusivity in a biofilm of *Pseudomonas aeruginosa* PAO1 to verify the published results. It is not clear whether the profiles of effective diffusivity are always linear. If a nonlinear variation of the relative effective diffusivity is found in the *Pseudomonas aeruginosa* PAO1 biofilms, then, perhaps, the mathematical model of stratified biofilm must account for that.

MATERIALS AND METHODS

Growing Biofilms

Experimental Setup

The experimental setup for growing the biofilms is shown in Fig. 2.1. Biofilms were grown in a flat plate flow reactor (8). The reactor had a polycarbonate channel 2.5 cm wide, 4.0 cm deep, and 34.5 cm long. The total volume of the reactor, including the tubing, was 150 ml. The tubing was supplied by Cole Parmer, Chicago, IL (Masterflex® 6402-16). Peristaltic pumps (7) manufactured by Cole Parmer were used to maintain the flow rates of the nutrient medium and the recycle streams. An in-line bacterial air vent filter (4) (Pall Gelman Laboratory, Ann Arbor, MI, USA) with a pore size of 0.45 μm was used for the air lines. The feed (1) and the waste (12) were stored in carboys which were autoclaved and sterilized. The frame grabber (10) was used to convert the analog image signal from the camera (9) into digital images which were stored in the computer (11).

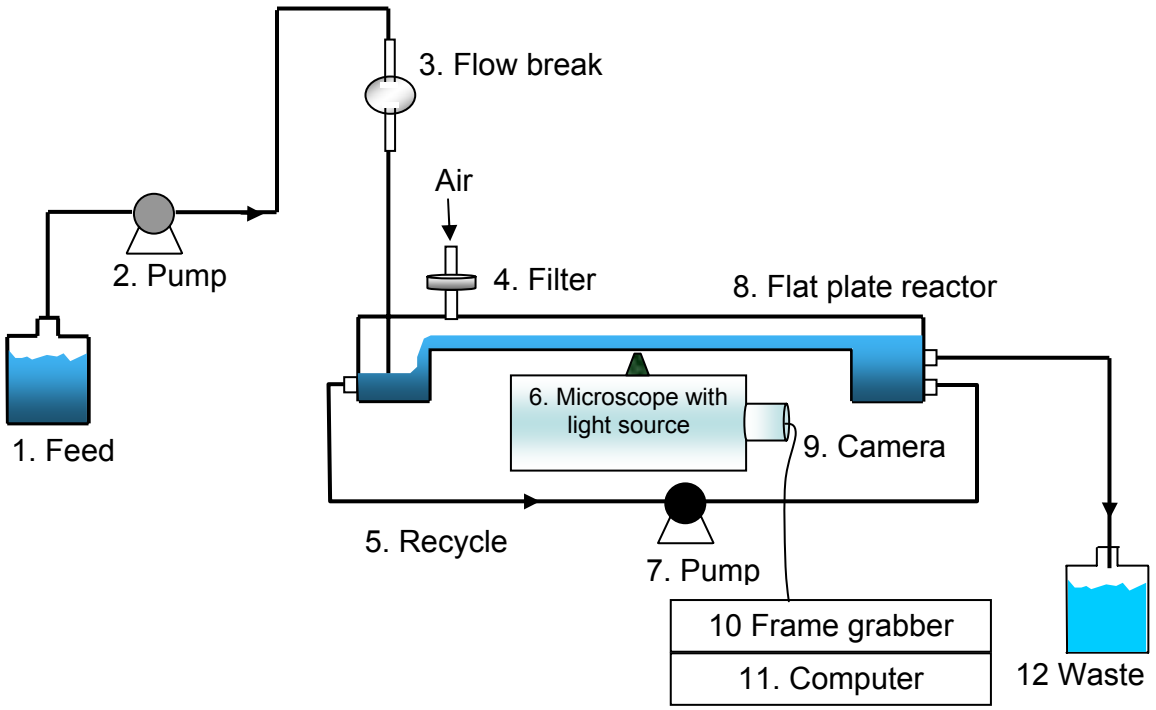

Fig. 2.1. Experimental setup for growing biofilms.

Reactor Preparation

The biofilms were grown on glass microscope slides placed on the bottom of the reactor. The width of the reactor and that of the microscope slides were equal so that the slides fit without any looseness. The surfaces of the slides (2.5 x 7.5 x 0.1 cm) were etched with 20% hydrogen fluoride for five seconds and then rinsed with deionized water before being placed on the bottom of the reactor. The etching helps to provide roughness on the glass slide surfaces, which facilitates better attachment of the biofilm. The etched slides were placed on the bottom of the reactor (etched side facing up) and held in position using stainless steel brackets to prevent the slides from moving or floating when the reactor was filled with nutrient medium or sterile water. To prevent contamination

of the reactor, it was sealed with 100% silicon rubber (Ace Hardware, Bozeman, MT). The reactor was sterilized using 20% bleach in water (Clorox®). The reactor was filled with 20% bleach in water and the bleach was left in the reactor for one hour. Then the bleach was drained from the reactor. To remove the residues of the bleach, the reactor was flushed with 20 L of autoclaved deionized water. To rinse the upper portions of the reactor, it was filled completely with sterile water and then drained. After at least five fill-and-drain cycles the sterile water was fed at a flow rate of 300 ml/h into the reactor overnight to remove any other possible bleach residues. The sterile water in the reactor was replaced with the growth medium just before inoculation.

Growth Medium

The medium composition is given in Table 1. The glucose and the yeast extract were dissolved in separate flasks (250 mL total volume) filled with 150 ml of water. Then they were autoclaved for 20 minutes at 121^{o}C. The autoclaved glucose and the yeast were added to the autoclaved growth medium to make the final concentrations in Table 1. The trace elements solution was added aseptically using a 0.2-μm syringe filter (Corning, NY). The medium pH was approximately 7.2. Trace elements (Table 2) were prepared in 1 L of 0.1 N HCl solution, and 1 mL of the trace elements solution was added to 1 L of the growth medium given in Table 1.

Table 1. The growth medium used to grow biofilms.

Component	Per liter of growth medium
Glutamic Acid (sodium salt)	0.1521 g
Glycerol	0.4604 g
Magnesium Sulfate	0.0492 g
Sodium Phosphate Monobasic	0.2759 g
Potassium Phosphate Dibasic	0.5051 g
Sodium Chloride	8.4738 g
Yeast extract	0.01 g
Glucose	1 g
Trace Elements	1 ml

Table 2. Trace elements.

Component	Concentration (mg/L)
$MnCl_2 \bullet 4H_2O$	527
$CuCl_2 \bullet 2H_2O$	228
$CoCl_2 \bullet 6H_2O$	317
$(NH_4)_6Mo_7O_{24} \bullet 4H_2O$	231
$Na_2B_4O_7 \bullet 10H_2O$	127
$ZnCl_2$	363
$CaCl_2$	3700
$FeCl_3$	2160

Reactor Inoculation and Operation

The frozen stock of *Pseudomonas aeruginosa* PAO1, which was genetically modified to express green fluorescence protein (GFP), was inoculated into a flask containing 100 ml of the growth medium. The GFP facilitated the acquisition of CLSM images of *Pseudomonas aeruginosa* PAO1. Then the flask

was placed in a shaker set at 150 rpm, at room temperature, for 24 hours. The biofilm reactor was inoculated with 30 ml of the microorganisms in the flask. A 30-ml syringe with a 16 gauge needle was used to transfer inoculum from the flask to the biofilm reactor. The inoculum was injected into the reactor through the line in which the air was entering the reactor. During the inoculation process the air flow to the reactor and the recycle were stopped, and the waste line was clamped. Twenty minutes after inoculation, the recycle and air flow to the reactor were restarted. Twelve hours after inoculation of the reactor a continuous feed of growth medium was started. The waste line was opened when the continuous feed was started. The feed flow rate was 0.4 ± 0.1 ml /min. Twice a day (early in the morning and late in the evening), the reactor was flushed with sterile deionized water to remove suspended microorganisms. The attached microscope ("6" in Fig. 2.1) was used to monitor biofilm formation.

Measurement Locations in the Biofilm

The dissolved oxygen, effective diffusivity measurements, and the CLSM imaging were done at the same location in the biofilm. A light microscopy image of the location is shown in Fig. 2.2. The eyepiece in the light microscope had a grid, which was used to identify 25 different equally spaced (100 μm) locations in the biofilm.

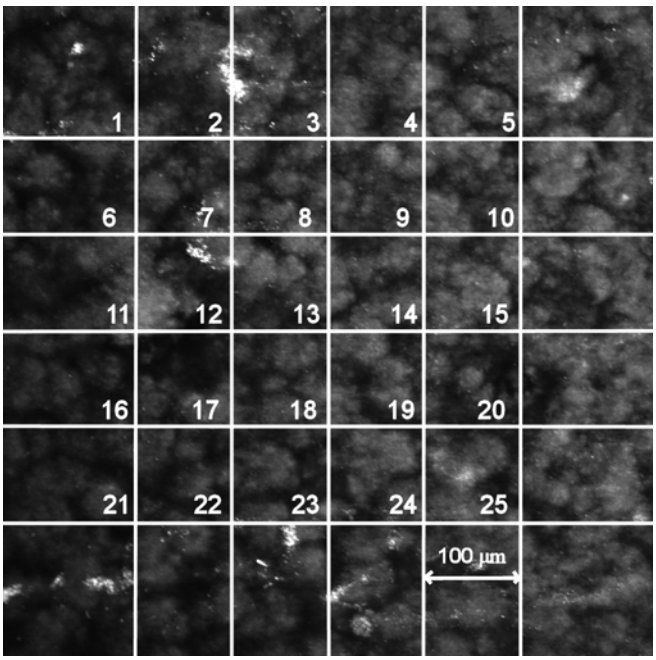

Fig. 2.2. Locations in the biofilm where dissolved oxygen concentration profiles and effective diffusivity profiles were measured and CLSM imaging was performed (1024 x 1024 pixels, or 675 µm x 675 µm).

Dissolved Oxygen Measurements: Principle and Procedures

Principle of Dissolved Oxygen Concentration Measurements

A schematic of the dissolved oxygen microelectrode is shown in Fig. 2.3. The microelectrode is made of a glass casing with a sharp tip covered with a silicone rubber membrane. The sensing/working electrode is made of gold-plated platinum. The typical tip diameter of the dissolved oxygen microelectrodes ranges from 10 µm to 20 µm. The silicone rubber membrane is permeable to gasses. The gasses in the vicinity of the microsensor tip diffuse through the silicon rubber membrane. The working electrode is polarized at -0.8 V against the

Ag/AgCl reference electrode to reduce the oxygen at the electrode surface (gold tip). Oxygen is electrochemically reduced at the cathode/working electrode according to the reaction in Eqn. 2.1. The reaction in Eqn. 2.2 occurs at the reference electrode, which is used as the anode/counter electrode. The overall reaction is given in Eqn. 2.3. The current generated by oxygen reduction at the cathode is correlated to the oxygen concentration in the vicinity of the microelectrode tip.

$$2e^- + \tfrac{1}{2} O_2 + H_2O \rightarrow 2\ OH^-$$

Eqn. 2.1

$$2Ag(s) + 2Cl^- \rightarrow 2AgCl + 2e^-$$

Eqn. 2.2

$$\tfrac{1}{2} O_2 + H_2O + 2Ag + 2Cl^- \rightarrow 2\ OH^- + 2AgCl$$

Eqn. 2.3

The polarization potential (-0.8V against Ag/AgCl) used for measurements is selected in the potential region which satisfies the limiting current condition for oxygen reduction. The limiting current is defined as the condition under which the current generated by the electrochemical reaction is controlled by the rate of the mass transfer of the electroactive component to the electrode. The limiting current is affected by various parameters, as given in Eqn. 2.4. For a particular fabricated microelectrode, all the terms on the right-hand side of Eqn. 2.4 are constant except the partial pressure, P_{O2} , of oxygen, which is controlled by the concentration of oxygen in the vicinity of the microelectrode tip. All of these constant terms can be combined into a single constant factor and can be easily calculated by a calibration process.

$$I = \frac{nFAD_m C_{O_2}}{Z_m}$$

Eqn. 2.4

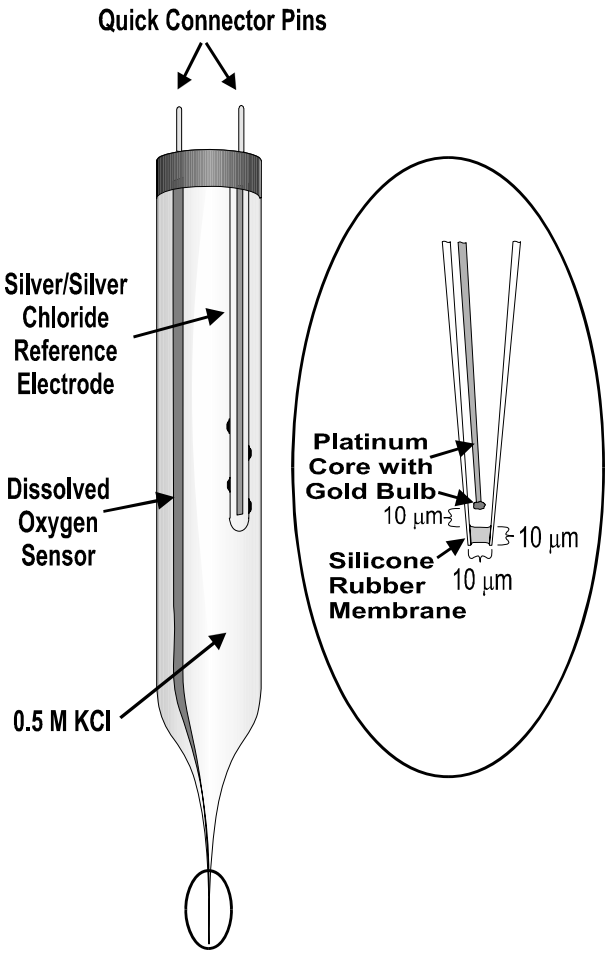

Fig. 2.3. Schematic of the dissolved oxygen microelectrode. (Reproduced from Microsensors Workshop Materials)

Calibration of the Dissolved Oxygen Microelectrode

The dissolved oxygen microelectrode must be calibrated before being used. Since the response current is related to the dissolved oxygen concentration linearly, two point calibration is sufficient (Revsbech and Jorgensen, 1986).

The calibration is performed by measuring the current at two different oxygen concentrations:

1) the saturation concentration (equilibrium concentration of oxygen in the air with water).

2) the zero oxygen concentration.

To obtain the zero oxygen concentration, nitrogen gas is bubbled in a beaker filled with water to remove the oxygen from the water. To obtain the saturation concentration, air is bubbled in a beaker filled with water to saturate the water with the oxygen in the air. The saturation dissolved oxygen concentration is 7.8 mg/L in water (at 25^{o}C and 1 atm pressure). However, the saturation concentration must be corrected for the pressure by multiplying 7.8 mg/L with the barometric pressure (atm) measured during the calibration.

The response time of the microelectrode is calculated as follows: The microelectrode is equilibrated with air (the concentration of oxygen is the same in air and in water); then it is immediately immersed in water which contains no oxygen (because it was continuously bubbled with nitrogen). The time elapsed

before the microelectrode reading is within 0.05 percent of the saturation value is considered the response time.

Fig. 2.4 shows the response of a dissolved oxygen microelectrode to an alternation in oxygen concentration between zero and 7.8 mg/L. The response time of this microelectrode was less than three seconds. Fig. 2.5 shows the calibration curve for this microelectrode.

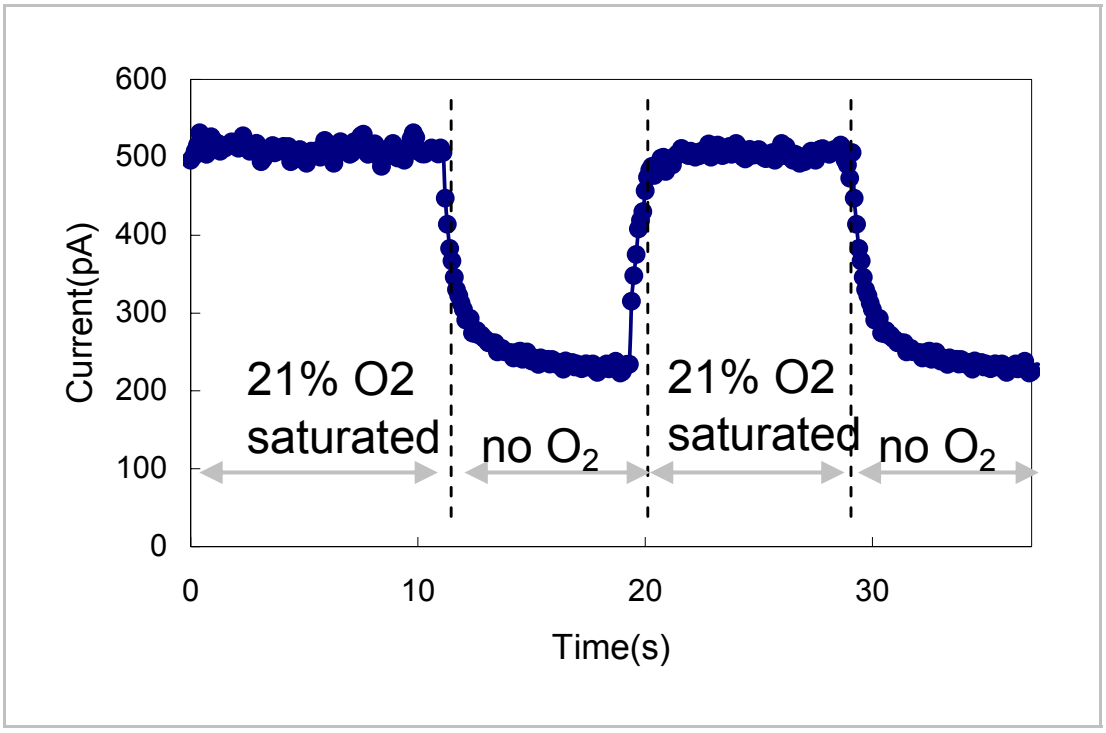

Fig. 2.4. Response of a dissolved oxygen microelectrode to an alternation in oxygen concentration between zero and 6.8 mg/L. Currents of 500 pA and 130 pA correspond to dissolved oxygen concentrations of 7.8 mg/L and zero mg/L, respectively. The time interval between measurements was 100 ms.

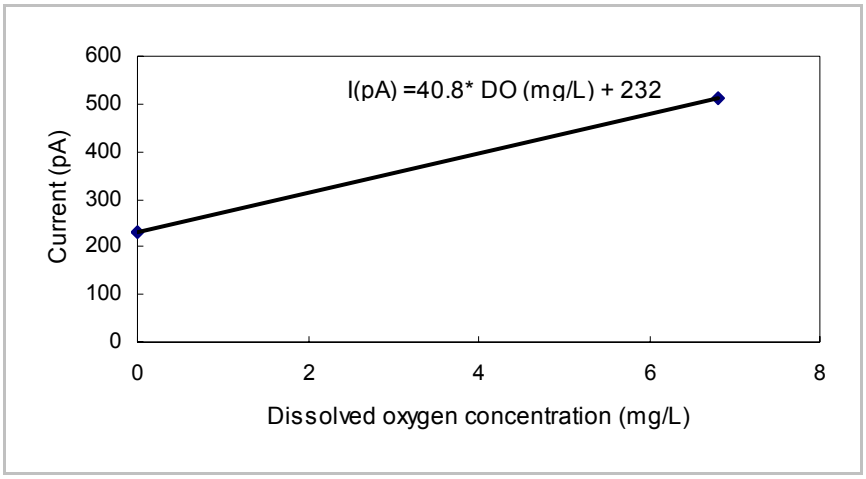

Fig. 2.5. Calibration curve of a dissolved oxygen microelectrode. The measured current is correlated with the dissolved oxygen concentration as
I(pA) =40.8* DO (mg/L) + 232

Dissolved Oxygen Concentration Measurements in Biofilms

The biofilms grown on the microscope slides in the reactors (Fig. 2.6) were moved carefully and placed in another clean reactor (identical to the reactor used to grow the biofilms) which is called a measurement reactor. The measurement reactor was located on top of an inverted microscope as shown in Fig. 2.6. The reactor was carefully filled with sterile growth medium, and exactly the same feed flow and recycle rates that were used to grow the biofilms were used to operate the reactor. We followed this procedure because a clean reactor provides better visibility of the biofilm and the microelectrode tip, and there is better control of the microelectrode. In addition, the biomass particles in the reactor which we used to grow the biofilms most likely would have stick to the tip of the microelectrode and caused a failure in the measurements.

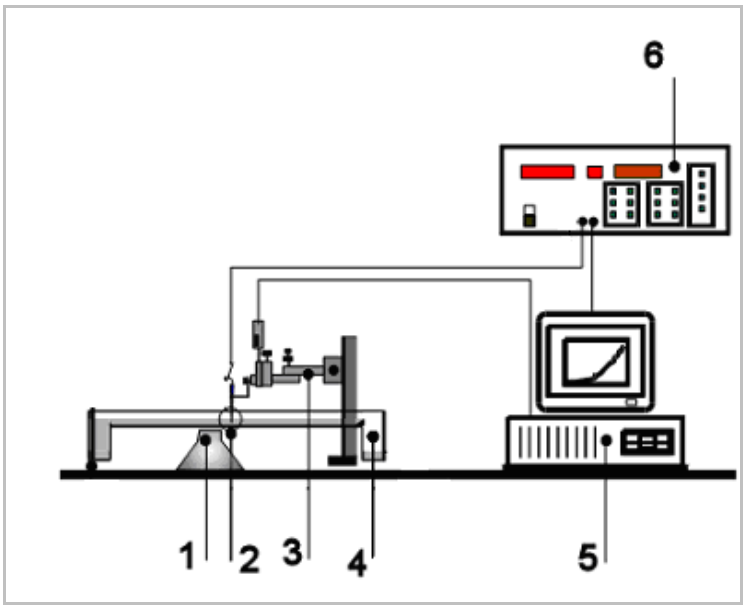

Fig. 2.6. Experimental setup used to perform dissolved oxygen microelectrode measurements: 1. inverted microscope, 2. microelectrode, 3. micromanipulator, 4. flat plate biofilm reactor, 5. data acquisition system, 6. picoammeter / DC voltage source. (Reproduced from Microsensors Workshop Materials)

The microelectrode was mounted on the stepper motor (Oriel 18503), which was attached to the micropositioner (Narishige Z-1). During the measurements the microelectrode was polarized at a potential of -0.8 V using a picoammeter/voltage source (HP 4140B). The stepper motor and the data acquisition system were controlled by custom-written software. Using the micromanipulator controlled by the software, the microelectrode was moved with a precision of 0.1 μm in the direction perpendicular to the biofilm surface.

The dissolved oxygen concentration profiles were measured at grid locations of a 4x4 grid matrix with a grid size of 100 μm. The locations of the

measurements are shown in Fig. 2.2. The step size used in the direction perpendicular to the biofilm surface was 10 μm.

Effective Diffusivity Measurements: Principle and Procedures

Local Mass Transfer Coefficient

The mass transport coefficient is measured using a limiting current technique. A single electrochemical reaction which proceeds at the maximum possible rate on the electrode surface is used for measuring the mass transport coefficient. Under mass-transfer-limiting conditions, the magnitude of the electrical current measured in the external circuit (Fig. 2.7) depends only on the mass transfer rate and is directly proportional to the mass transfer coefficient of the electrode (Yang and Zbigniew 1995). The tip of the microelectrode forms a microsink for the electroactive species (ferricyanide) purposely added to the biofilm reactor.

The measured limiting current is directly proportional to the local mass transfer rate to the electrode. The magnitude of the limiting current is dependent on a combination of all factors influencing the local mass transport rate, e.g., local hydrodynamics and the local structure of the biofilms. The local mass transfer coefficient calculated from the measured limiting current of the microelectrode surface is related to the local effective diffusivity, which is a function of local hydrodynamics and local biofilm structure.

The redox system (Eqn. 2.5) consisting of ferri-ferrocyanide is used for measuring the mass transport coefficient in biofilms (Yang and Zibigniew 1995). The polarization potential is increased until the concentration of $Fe(CN)^{4-}_6$ at the electrode surface reaches zero (C_s = 0). The current corresponding to a zero surface concentration of the reacting species is the limiting current. The flux of the ferricyanide ion, J, to the surface of the microelectrode with sensing area A is related to limiting current I according to Eqn. 2.6. The flux is related to the mass transfer coefficient according to Eqn. 2.7.

By combining Eqn. 2.6 and Eqn. 2.7 the relationship between mass transfer coefficient and limiting current can be found (Eqn. 2.8).

$$Fe(CN)_6^{-3} + e^- \rightarrow Fe(CN)_6^{-4} \qquad \text{Eqn. 2.5}$$

$$J_f = \frac{I}{nAF} \qquad \text{Eqn. 2.6}$$

$$J_f = k_f(C_0 - C_s) \qquad \text{Eqn. 2.7}$$

$$k_f = \frac{I}{nAFC_0} \qquad \text{Eqn. 2.8}$$

Local Effective Diffusivity

The mass transfer boundary layer thickness is not taken into account in the case of mass transfer coefficient, but in the case of local effective diffusivity it is. Local effective diffusivity can be measured by cathodically polarizing a platinum surface located at the tip of the microelectrode. The electroactive chemical is reduced at the tip of the microelectrode. This technique is useful only

if there is only one electroactive species present in the solution. The experimental setup for measuring local effective diffusivity is shown in Fig. 2.7.

To measure the local effective diffusivity, ferricyanide ($Fe(CN)_6^{-3}$) was used as the electroactive species (Beyenal et al. 1999). The growth medium was replaced with the ferricyanide solution. When the microelectrode is cathodically polarized against a reference electrode, the reaction in Eqn. 2.5 occurs, leading to an overall electric current flow in the circuit. Increasing the polarization potential increases the current until the concentration of the ferricyanide decreases to zero at the microelectrode surface. The current at this condition is called the limiting current. The flux of ferricyanide to the electrode surface, J (moles/m^2/s), is calculated according to Eqn. 2.6. From Fick's first law (Eqn. 2.9) the flux is also related to the diffusivity of ferricyanide (D_{CN}) at the limiting current (C_s=0). From Eqn. 2.11, the limiting current depends on the diffusivity of the electroactive species in the vicinity of the microelectrode tip. The limiting current density (I/A) is related to the local effective diffusivity of ferricyanide according to Eqn. 2.13 (Beyenal and Lewandowski 2000).

$$J_f = D_{CN}\frac{C_o - C_s}{\delta} = D_{CN}\frac{C_o}{\delta}$$

Eqn. 2.9

$$J_f = \frac{I}{nAF} = D_{CN}\frac{C_o}{\delta}$$

Eqn. 2.10

$$I = D_{CN}\frac{C_o}{\delta}nAF$$

Eqn. 2.11

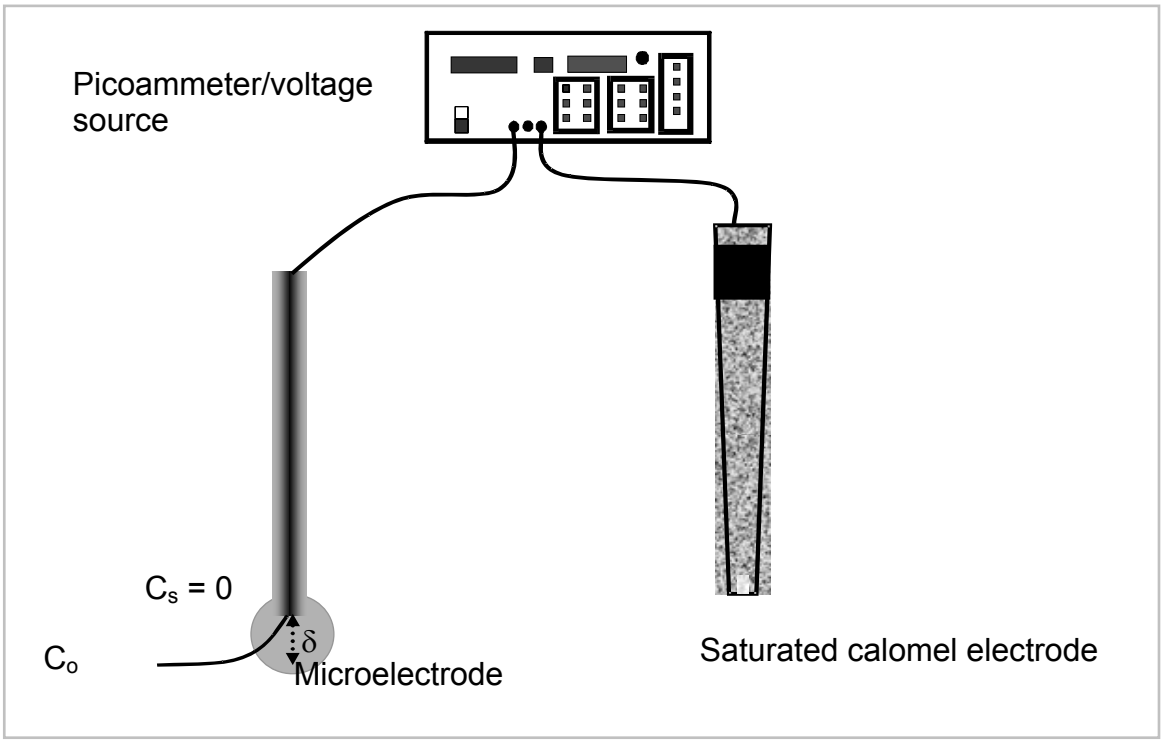

Fig. 2.7. Experimental setup for measuring the local mass transfer coefficient and local effective diffusivity. (Reproduced from Microsensors Workshop Materials)

To obtain Eqn. 2.13 Beyenal and Lewandowski (2000) first measured the diffusivity of ferric cyanide in agar gels of different densities (Eqn. 2.12). Then they found the correlation between the limiting current density and the density of the agar gels by measuring the limiting current densities in agar layers of different known densities. Using these two quantifications Beyenal and Lewandowski (2000) arrived at Eqn. 2.13.

$$D_{ag} = 3.72 * 10^{-10} - 5.43 * 10^{-12} X_{ag} + 2.79 * 10^{-14} * X_{ag}^{\ 2}$$

Eqn. 2.12

$$D_{ag} = 1.12 * 10^{-10} + 3.69 * 10^{-12} \frac{I}{A}$$

Eqn. 2.13

Local Effective Diffusivity
Measurements in Biofilms

The experimental setup for the local effective diffusivity measurement is shown in Fig. 2.6. This is the same reactor that was used to measure the dissolved oxygen concentrations. However, it is modified to measure the local effective diffusivity in the biofilm. Just before the local effective diffusivity measurements, the nutrient solution in the biofilm reactor was replaced with an electrolyte. First, the reactor was slowly flushed with 0.2 M KCl to remove the nutrient solution. Then the 0.2 M KCl was replaced with an electrolyte solution of 0.025 M $K_3Fe(CN)_6$ in 0.2 M KCl. This procedure does not affect the biofilm structure (Yang and Lewandowski 1995; Beyenal and Lewandowski 2000). The ferricyanide solution was recycled for two hours, until it reached equilibrium with the biofilm. The microelectrode was mounted on the stepper motor (Oriel 18503), which was attached to the micropositioner (Narishige Z-1). During the measurements, the microelectrode was polarized at a potential of -0.8 V using the picoammeter/voltage source (HP 4140B). The stepper motor and the data acquisition system were controlled by custom-written software. Using the software, the microelectrode can be moved with a precision of 0.1 μm in the direction perpendicular to the biofilm surface.

The local effective diffusivity profiles were measured at grid locations of a 4x4 grid matrix with a grid size of 100 μm. The locations of the measurements are shown in Fig. 2.2. The step size used in the direction perpendicular to the biofilm surface was 10 μm.

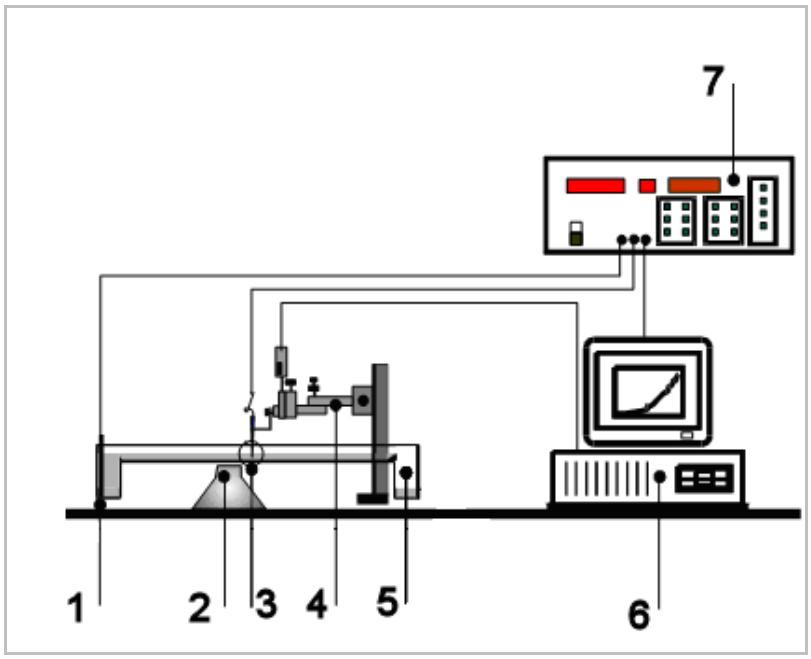

Fig. 2.8. Experimental setup used to perform microelectrode measurements: 1. reference electrode; 2. inverted microscope; 3. microelectrode; 4. micro-manipulator; 5. flat plate biofilm reactor. 6. data acquisition system; 7. pico-ammeter / DC voltage source. (Reproduced from Microsensors Workshop Materials)

Calculation of Local Relative Effective Diffusivity

The local effective diffusivity values were divided by the molecular diffusivity of ferricyanide in the electrolyte solution, $D_{CN}=7 \times 10^{-10}$ m^2/s (Gao et al. 1995), to calculate the relative effective diffusivity.

Calculation of Surface Averaged Parameter Values

The surface averaged dissolved oxygen concentration (C_{SA}) for a given distance (z) from the bottom is calculated by averaging the local values (25

values) (Eqn. 2.14). The surface averaged relative effective diffusivity (D_{SA}) for a given distance (z) from the bottom is calculated by averaging the local relative effective diffusivities (Eqn. 2.15).

$$C_{SA} = \sum_{i=1}^{25} \frac{C_{Li}}{25}\bigg|_Z$$

Eqn. 2.14

$$D_{SA} = \sum_{i=1}^{25} \frac{D_{Li}}{25}\bigg|_Z$$

Eqn. 2.15

Calculations of Standard Deviation and Coefficient of Variation

The standard deviation and coefficient of variation (CV) of the surface averaged dissolved oxygen concentration were calculated according to Eqn. 2.16 and Eqn. 2.17, respectively. These parameters were calculated so as to quantify the variation of dissolved oxygen concentration in any given layer in the biofilm.

$$C_{SD} = \sqrt{\frac{\sum_{i=1}^{25} (C_{Li} - C_{SA})^2}{25}}$$

Eqn. 2.16

$$C_{CV} = \frac{C_{SD} * 100}{C_{SA}}$$

Eqn. 2.17

The standard deviation and coefficient of variation of the surface averaged relative effective diffusivity were calculated according to Eqn. 2.18 and Eqn. 2.19, respectively. These parameters were calculated so as to quantify the variation of

relative effective diffusivity in any given layer in the biofilm. The higher the value of CV, the higher the variability, which can also be related to the heterogeneity of the biofilm.

$$D_{SD} = \sqrt{\frac{\sum_{i=1}^{25} (D_{Li} - D_{SA})^2}{25}}$$

Eqn. 2.18

$$D_{CV} = \frac{D_{SD} * 100}{D_{SA}}$$

Eqn. 2.19

Confocal Laser Scanning Microscopy

Biofilm is made up of a three-dimensional distribution of biomass. To quantify the biofilm structure, a three-dimensional image of the biofilm must be obtained. Confocal laser scanning microscopy (CSLM) can be used to obtain the layer images of the biofilms, and these layer images can be used to quantify the structure of the biofilm. A schematic of CLSM is shown in Fig. 2.9. In CSLM, a laser is used as the light source (7) for the CLSM imaging. The laser (7) beam is focused by using a lens (6) and a laser pinhole (4). The laser beam is reflected by a beam splitter (2) on the object in the focal plane. The main function of the beam splitter (2) is to separate the laser light from the emitted light coming from the sample. When the biofilm is exposed to a laser of a particular wavelength, substances (in our case the GFP) in the biofilm are excited and emit a response emission of different wavelengths. Then the beam splitter allows only that

wavelength which corresponds to the “response emission” to reach the detector pinhole (3). This emitted light passes through the pinhole (3) and is then recorded by the detector (1), i.e. the photomultiplier tube (PMT).

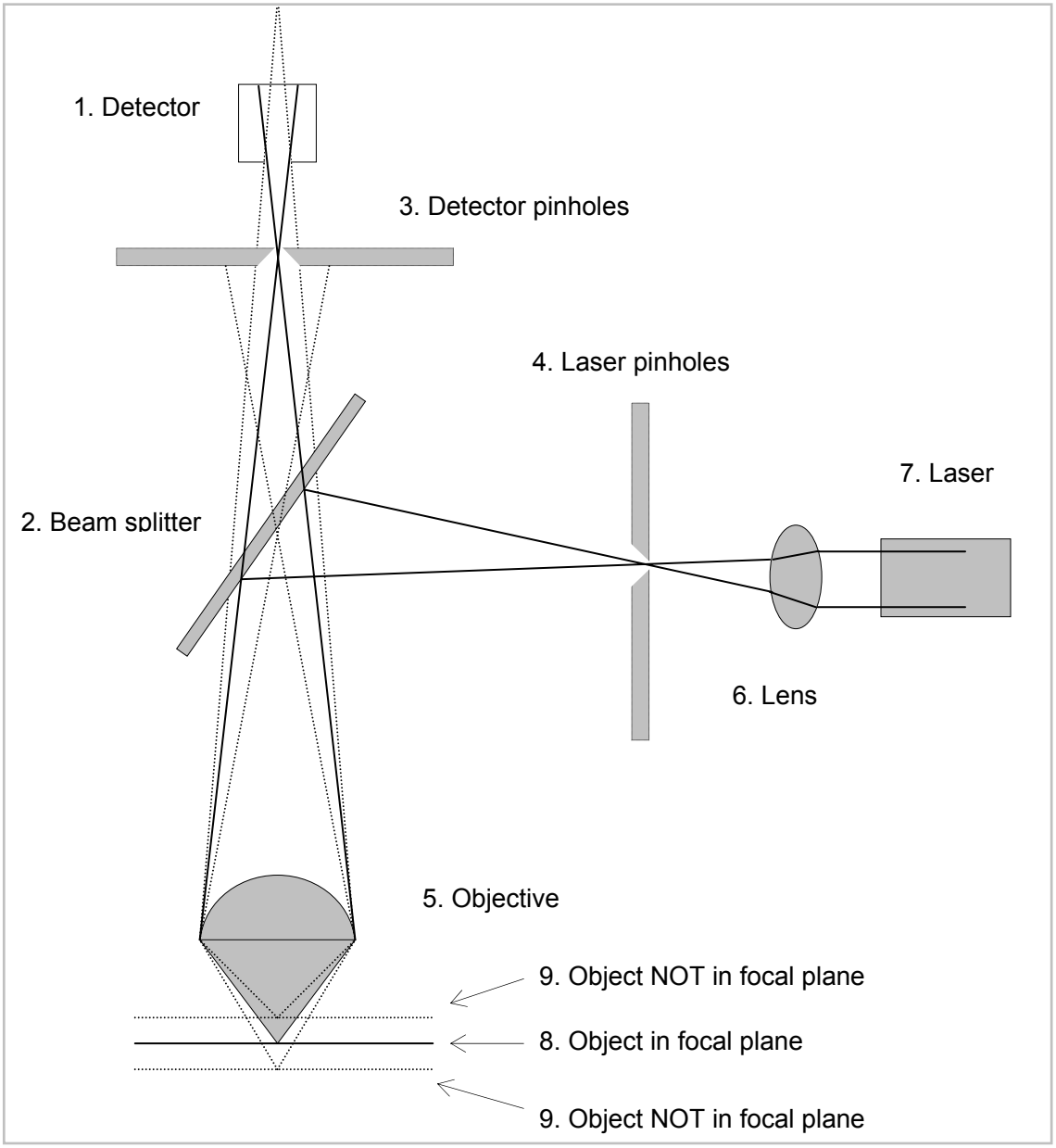

Fig. 2.9. Schematic of confocal laser scanning microscope principle (adapted from Leica concofal microscopy systems® http://www.confocal-microscopy.com/website/sc_llt.nsf)

The response emission light from the object that is not in the plane of focus is rejected by the pinhole (3) placed before the light detector (1). Thus, by scanning the laser through different x-y locations on a layer of the biofilm, the whole layer can be imaged. The depth of the focal plane is dependent on the wavelength of the laser, the aperture diameter of the objective and the diameter of the diaphragm. The photomultiplier, which acts as the light detector (1), is used to transform a light signal into an electrical signal that is displayed by the computer.

CLSM Imaging of Pseudomonas Aeruginosa PAO1

The biofilms, grown on glass slides, in which dissolved oxygen concentration profiles were measured, were carefully removed from the flat plate reactor and then placed in a Petri dish with the biofilms facing up. The Petri dish was partially filled with the growth medium. Light microscopy, which was a part of the Leica upright confocal laser microscopy, was used to identify the location in the biofilm where the microelectrode measurements were done. Then CLSM was performed at that location using a Leica upright confocal scanning microscopy system (DM RXE).

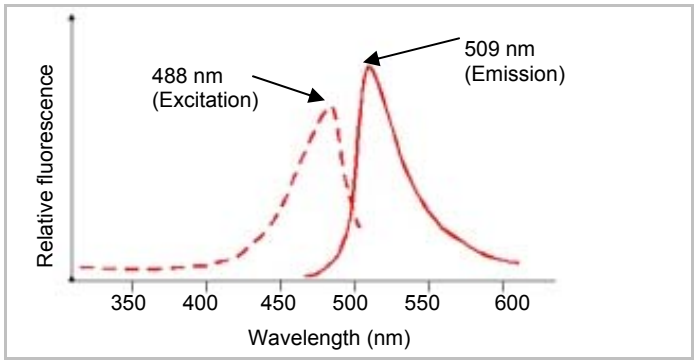

Fig. 2.10. The excitation and the emission spectra of green fluorescence protein (GFP) (Image obtained from http://www.biotek.com).

Since the *Pseudomonas aeruginosa* PAO1 in the biofilm contained GFP, the appropriate excitation and emission wavelengths corresponding to GFP were used to obtain the CLSM images. From Fig. 2.10, it is seen that GFP, when excited with a light source of 488 nm, emits a response light of 509 nm wavelength. Thus, for this experiment a laser source of 488 nm was used and a detector (1) was configured through the software to capture the 509-nm response light. An objective of 10x magnification was chosen for the CLSM imaging.

The step size perpendicular to the biofilm surface and the range of the z scan were selected using the CLSM interface software provided by Leica. A z step size of 10 μm was used and the z scan was done from 0 μm (bottom) to 110 μm (top) of the biofilm. The layered images obtained are shown in Fig. 2.11

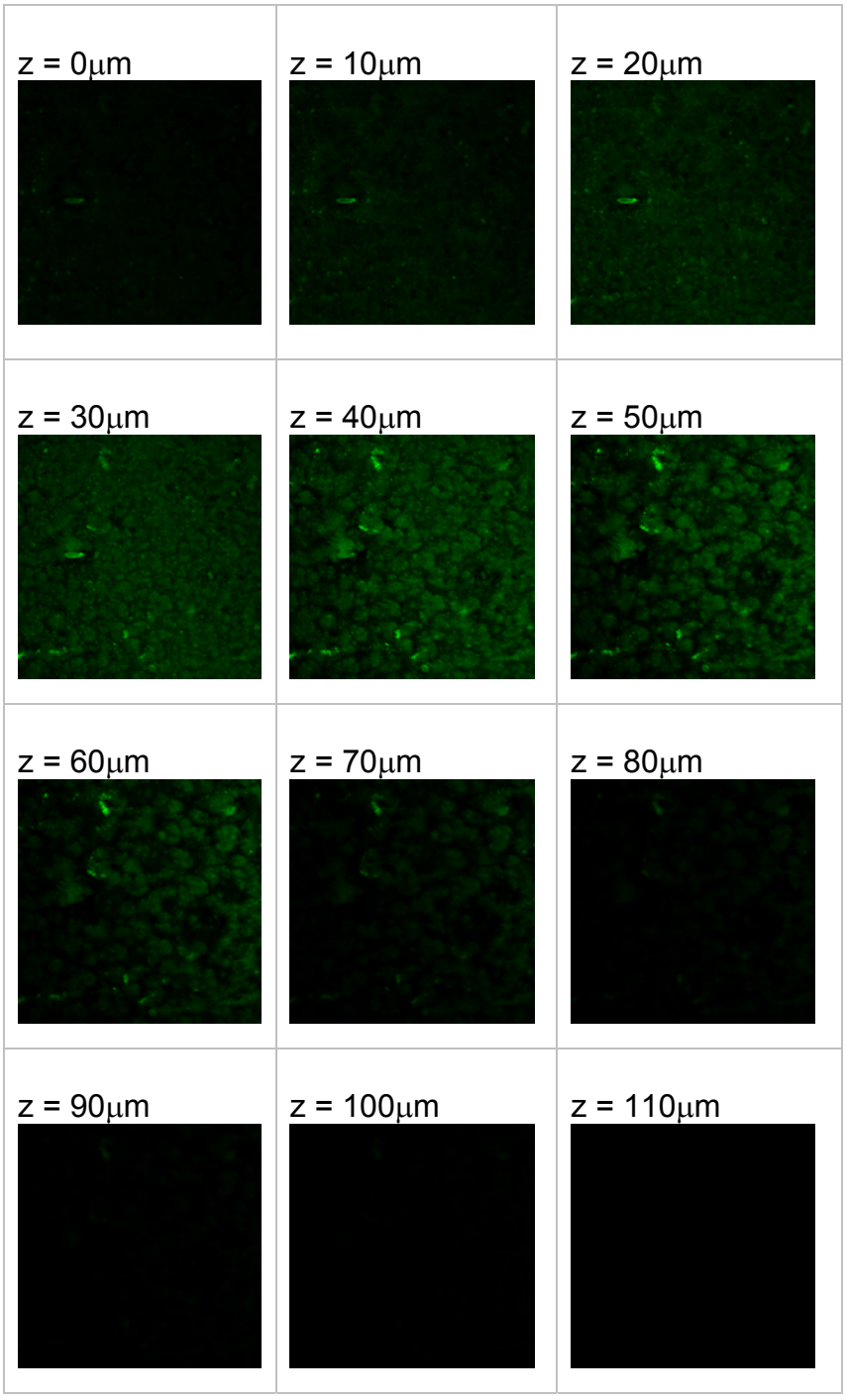

Fig. 2.11. Layered images of *Pseudomonas aeruginosa* PAO1 biofilm taken using CLSM. Image size is 1024x1024 pixels and 1 pixel = 0.66 μm.

Calculations of Areal Porosity
and Standard Deviation

Each image (layer) was segmented into nine grid segments. The areal porosity of each segment was calculated using the ISA-2 software. The average areal porosity of all the segments in an image was calculated and then the standard deviation of porosity in that layer was calculated according to Eqn. 2.20.

$$AP_{SD} = \sqrt{\frac{\sum_{q=1}^{9} (AP_q - AP)^2}{9}}$$

Eqn. 2.20

$$AP_{CV} = \frac{AP_{SD} * 100}{AP}$$

Eqn. 2. 21

RESULTS AND DISCUSSION

The goals of this study were to (1) correlate the dissolved oxygen concentration in a biofilm with relative effective diffusivity, (2) correlate the dissolved oxygen concentration in the biofilm with areal porosity, and (3) correlate the relative effective diffusivity with the areal porosity. To accomplish this we designed and executed a series of measurements in a biofilm of *Pseudomonas aeruginosa* PAO1 grown in a flat plate reactor. The results of these measurements are shown and interpreted in the following section.

Dissolved Oxygen Concentration Profiles

Fig. 3.1 shows the dissolved oxygen concentration profiles measured at 25 different locations in the biofilm (Fig. 2.2). The profile measurements were carried out at each of the grid points of the 4x4 lateral grid shown in Fig. 2.12. Each profile was obtained by measuring the dissolved oxygen concentration every 10 μm across the biofilm. Curves with higher dissolved oxygen concentration are obtained whenever the measurement is made at locations where there is no biofilm present. From the results in Fig. 3.1, for each layer of the biofilm we computed the average local dissolved oxygen concentrations and plotted the results measured at the same distances from the bottom of the biofilm in Fig. 3.2.

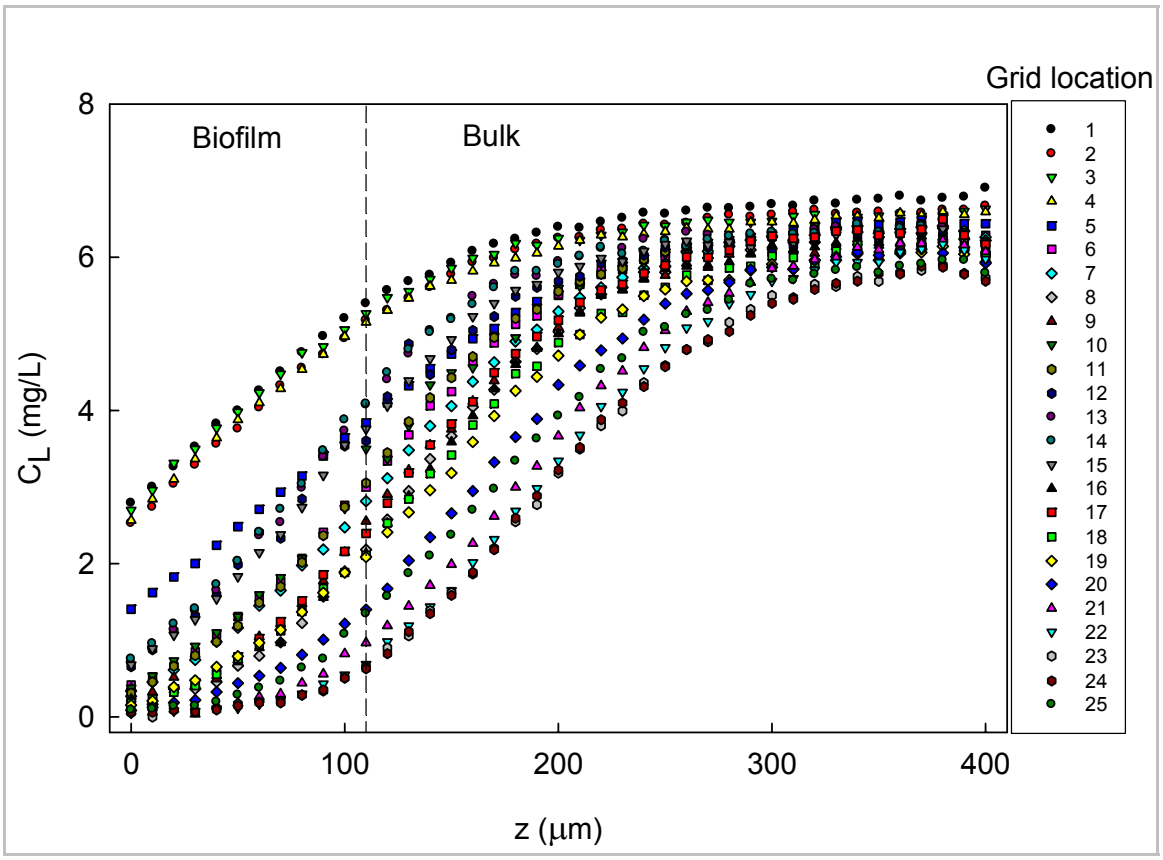

Fig. 3.1. Dissolved oxygen concentration profiles measured at 25 different locations (Fig. 2.2) in the biofilm.

The error bars in Fig. 3.2 show the standard deviation of the dissolved oxygen concentration in each layer. These bars do not represent the uncertainty related to the errors in measurement, however. They represent the variation in the distribution of oxygen concentration in the individual layers. The envelope formed by the standard deviations indicates that the variation in oxygen concentration (chemical heterogeneity) increases as the bottom of the biofilm is approached. The dissolved oxygen concentration varies inside the biofilm (Fig. 3.1) because biomass and biofilm activity are not evenly distributed inside the

biofilm. The variation in dissolved oxygen concentration in each layer is quantified by calculating the standard deviation of the local dissolved oxygen concentration (error bars in Fig. 3.2).

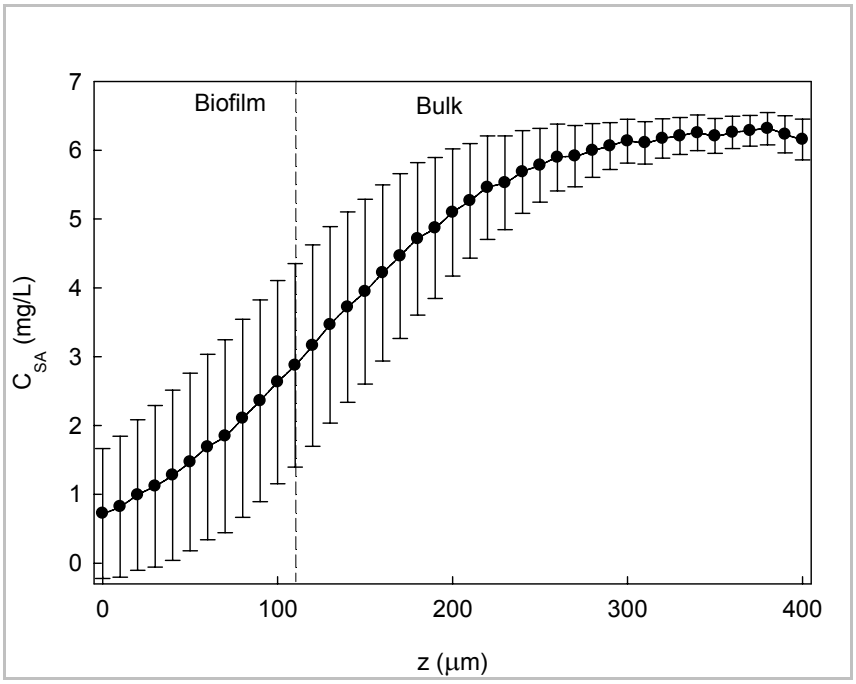

Fig. 3.2. Surface averaged dissolved oxygen concentration (calculated using data from Fig. 3.1) decreases towards the bottom of the biofilm. The error bars show the standard deviation of the dissolved oxygen concentration in each layer.

To determine the degree of variation in dissolved oxygen concentration between layers, the coefficient of variation was also computed and plotted against distance from the bottom of the biofilm (Fig. 3.3). The coefficient of variation is a standard deviation normalized with respect to the average, and is a more objective indicator of the distribution of oxygen in the biofilm. The data in Fig. 3.3 show that the coefficient of variation is linearly related to the distance: the closer to the bottom, the lower the coefficient of variation. This trend can be

interpreted as a result of nutrient diffusion resistance in the biofilm. The top layer of the biofilm has direct access to the bulk nutrient, so any lateral variation in dissolved oxygen concentration occurring there is quickly compensated for by the nutrient flux from the bulk solution. In contrast, the nutrient supply to the lower layers of the biofilm is limited because the nutrients must diffuse through the layers of the biofilm.

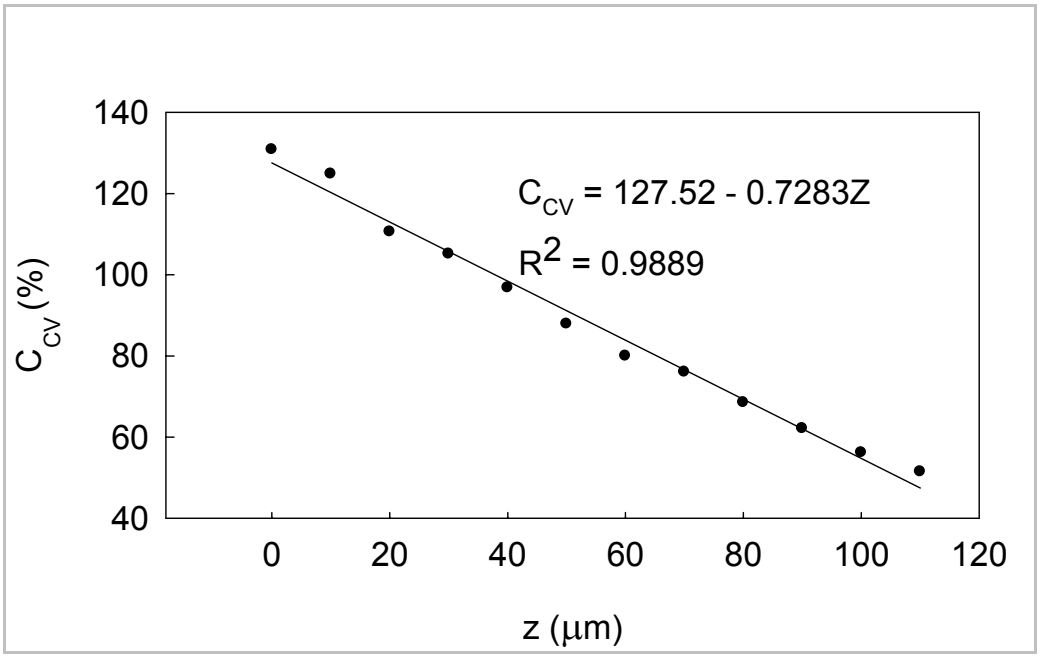

Fig. 3.3. The coefficient of variation in dissolved oxygen concentration (C_{CV}) plotted against the distance from the bottom of the biofilm (z).

Since the paths of diffusion inside the biofilm are convoluted because of biofilm porosity, the differences among local concentrations of oxygen increase near the bottom. The results in Fig. 3.4 corroborate these observations. It is interesting to note that the profile of the coefficient of variation in Fig. 3.3 is surprisingly linear. Fig. 3.4 shows the local dissolved oxygen concentration in

each layer of the biofilm. The roughness of the surfaces in the plots increases towards the bottom of the biofilm, indicating that the variation in local dissolved oxygen concentration increases towards the bottom of the biofilm.

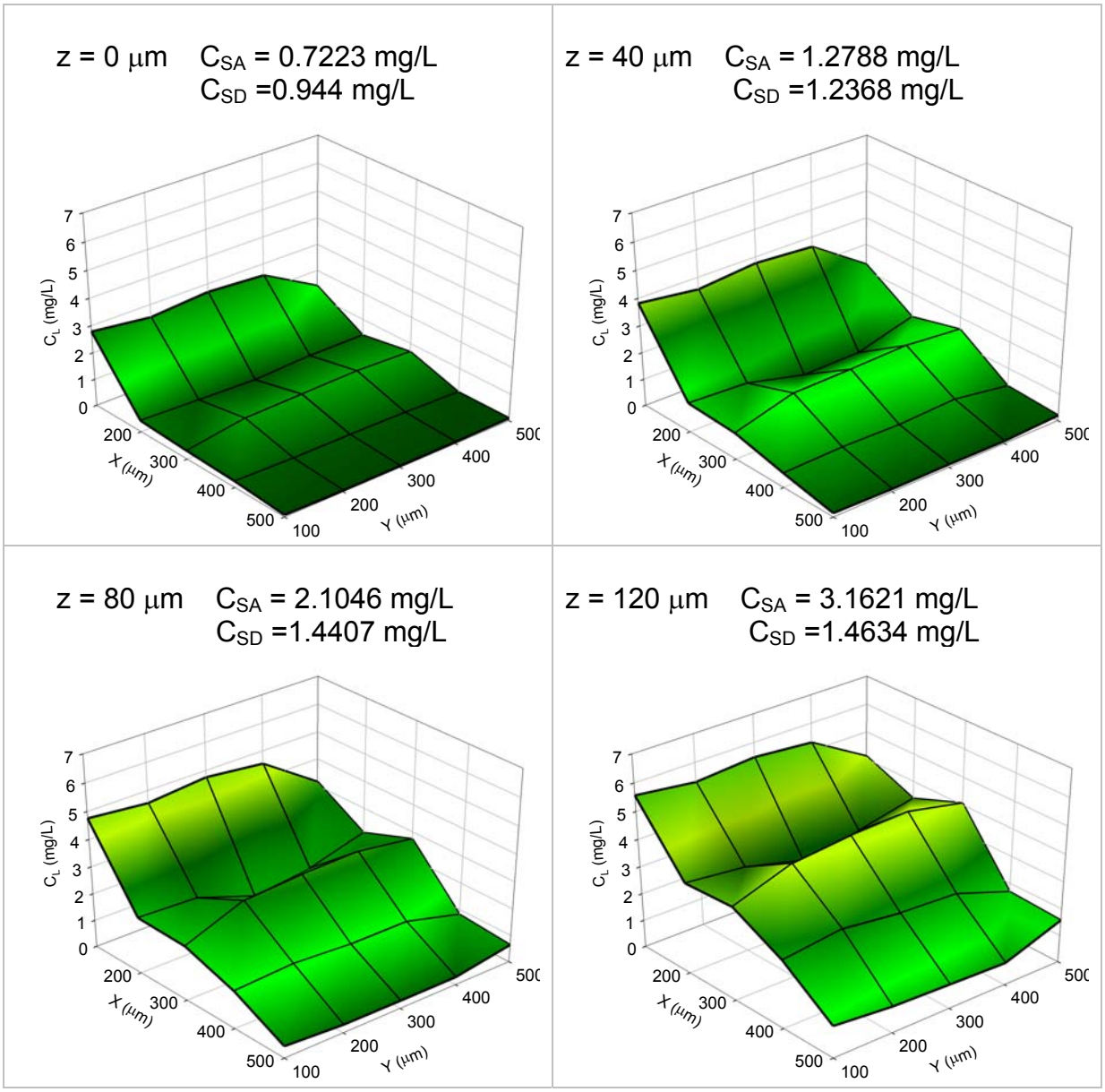

z = 160 μm C_{SA} = 4.2182 mg/L
C_{SD} =1.2795 mg/L

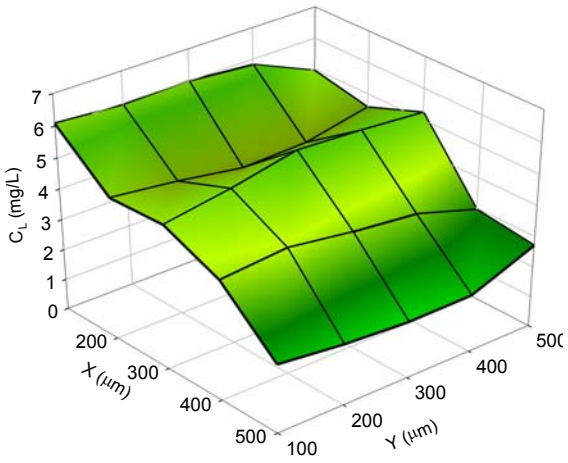

z = 200 μm C_{SA} = 5.0966 mg/L
C_{SD} =0.9237 mg/L

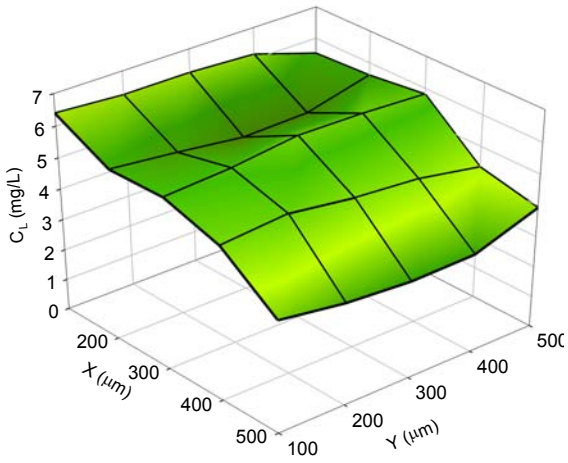

z = 240 μm C_{SA} = 5.6857 mg/L
C_{SD} =0.6007 mg/L

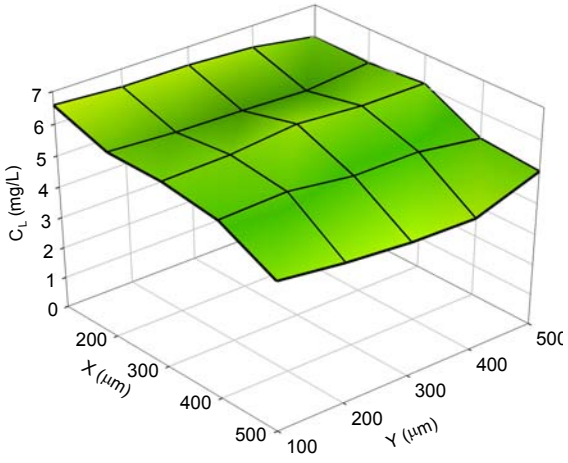

z = 280 μm C_{SA} = 5.9964 mg/L
C_{SD} =0.3915 mg/L

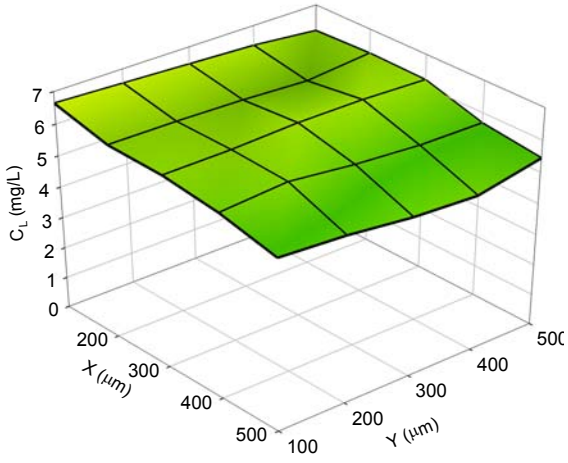

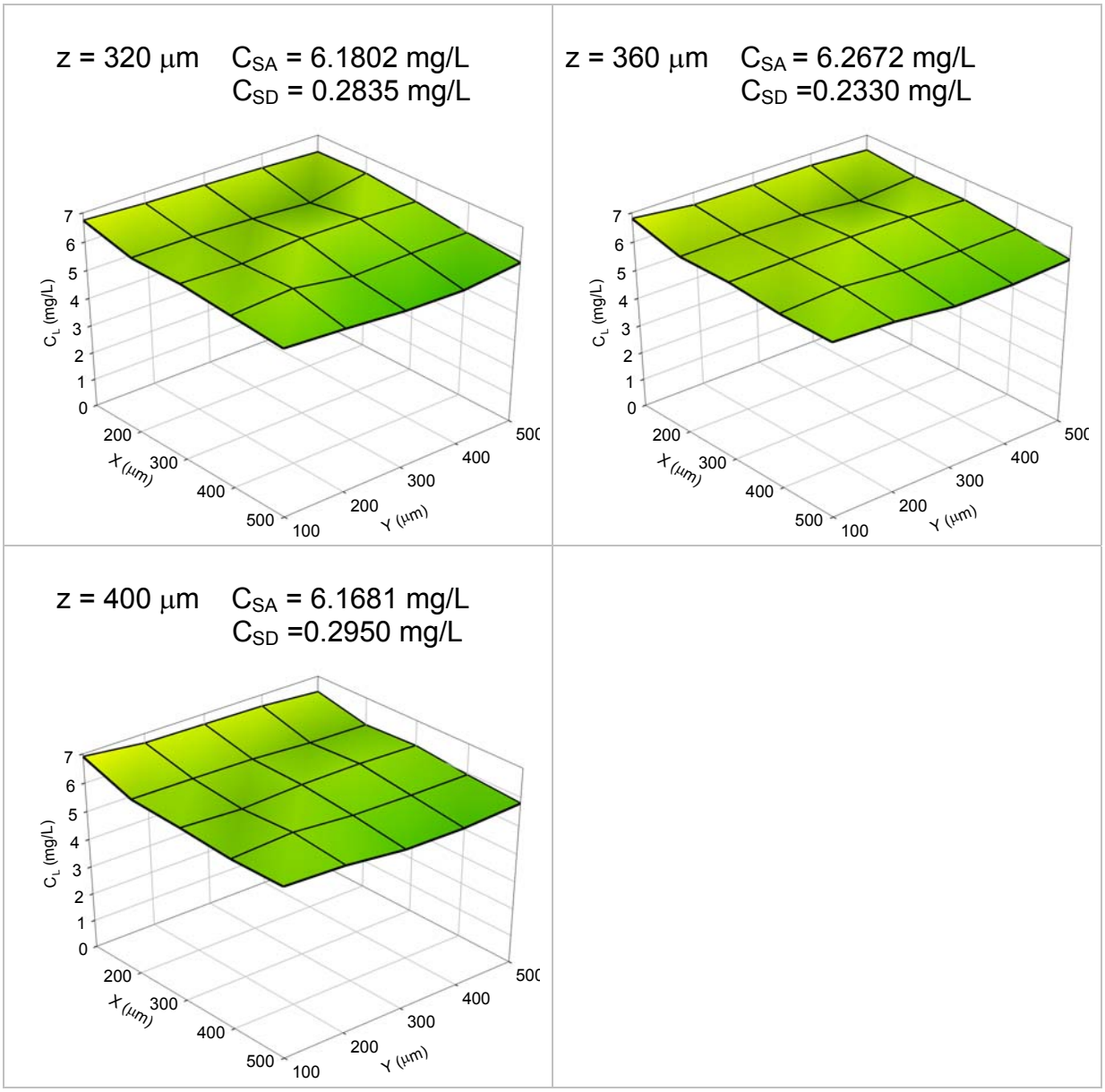

Fig. 3.4. Surface plot of dissolved oxygen concentrations in different layers in the biofilm. Where: C_{SA} is the surface averaged dissolved oxygen concentration (mg/L) and C_{SD} is the standard deviation of the local dissolved oxygen concentration. z = represents the bottom of the biofilm.

Local Relative Effective Diffusivity Profiles

Fig. 3.5 shows the variation in local relative effective diffusivity with distance from the bottom of the biofilm, measured at the 25 grid locations in the biofilm shown in Fig. 2.2.

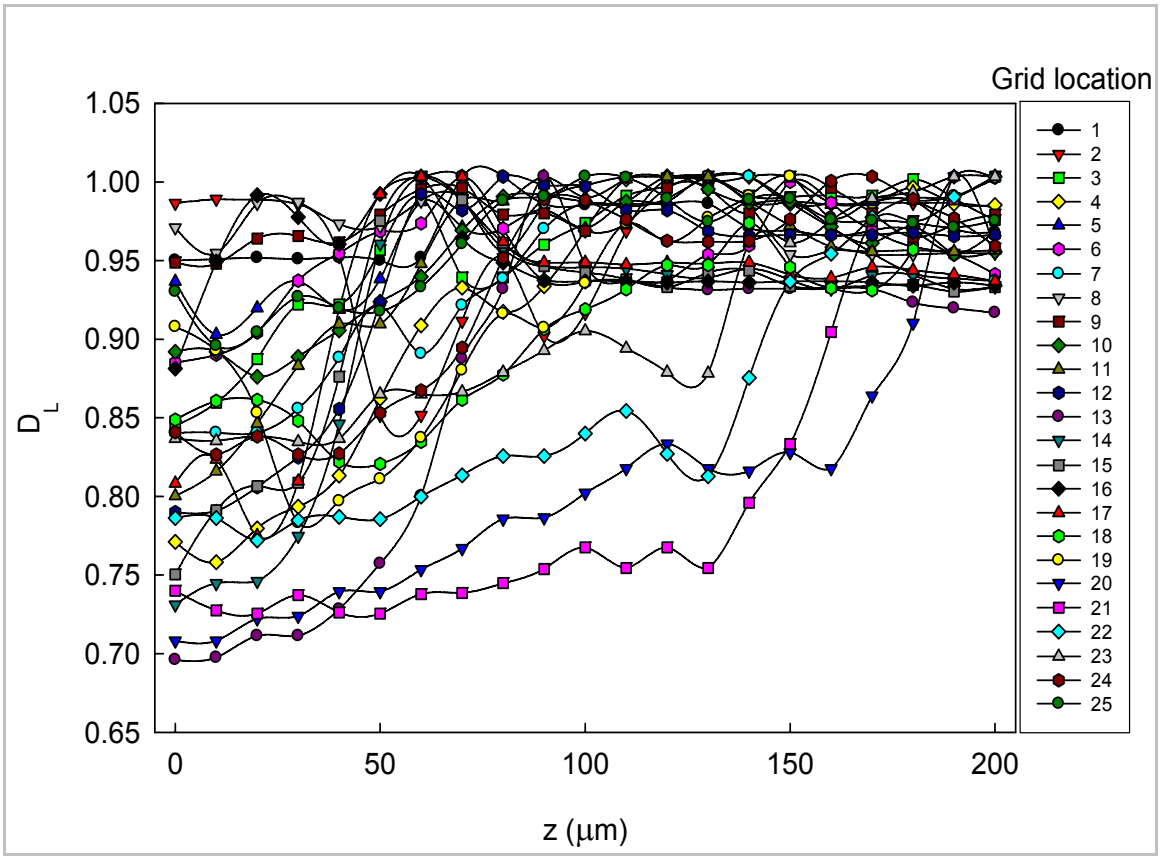

Fig. 3.5. Local relative effective diffusivity profiles measured at the 25 locations shown in Fig. 2.2.

The profile of the dissolved oxygen concentration (Fig. 3.1) is much more regular than the profile of the relative effective diffusivity (Fig. 3.5). This difference is caused by the fact that large differences in concentration of oxygen among locations are quickly reduced because of oxygen diffusion, while large

differences in diffusivity among locations, caused by differences in biomass density, cannot be reduced easily.

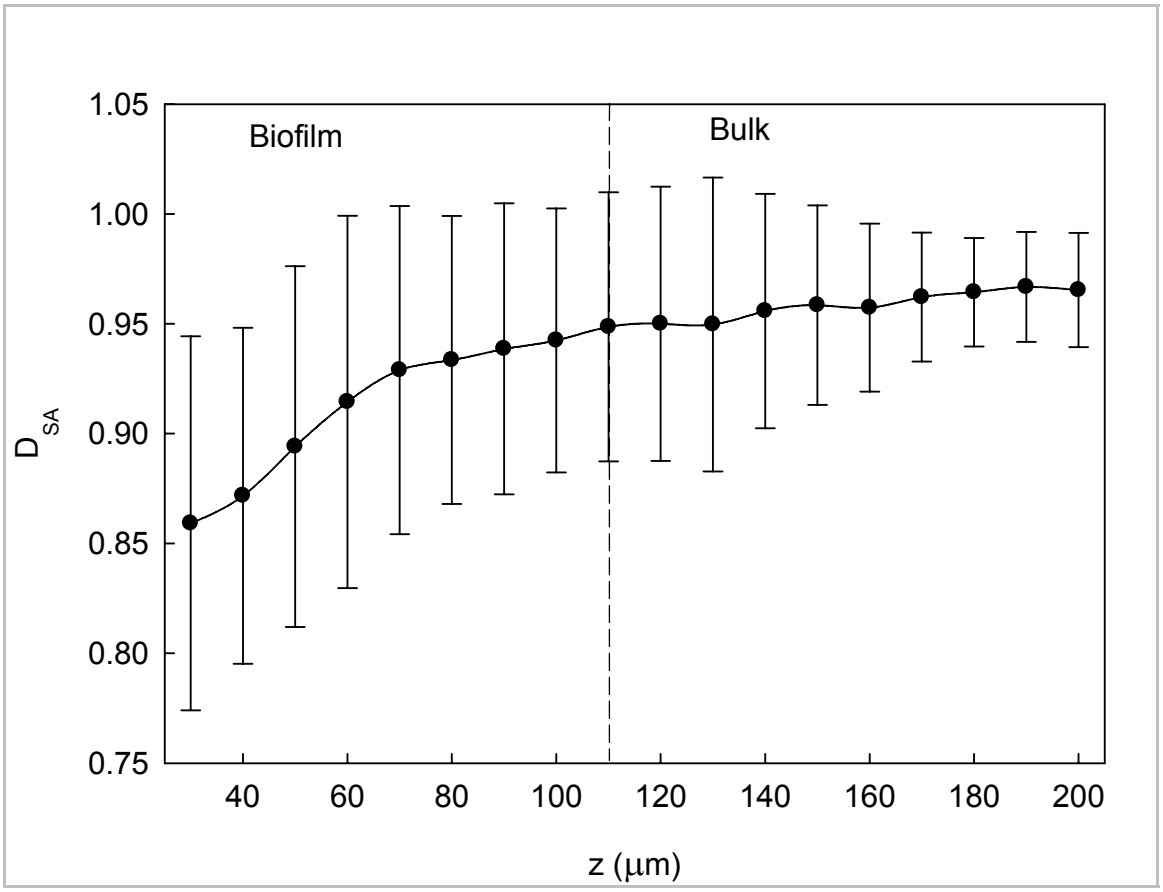

Fig. 3.6. The variation in surface averaged relative effective diffusivity with distance (calculated using the data from Fig. 3.5).

Since the local relative effective diffusivity varies among locations within each layer of the biofilm, as shown in Fig. 3.5, the surface averaged relative effective diffusivity (D_{SA}) and standard deviation from D_{SA} were computed (Fig. 3.6) for each layer of the biofilm. The plot of D_{SA} vs. distance is more regular and shows a trend that can be interpreted. The local relative effective diffusivity, D_{SA}, decreases toward the bottom of the biofilm while the standard deviation of the

local relative effective diffusivity increases toward the bottom of the biofilm (Fig. 3.6); the coefficient of variation increases linearly towards the bottom of the biofilm (Fig. 3.7).

The flux is linearly related to the diffusivity (D_{SA}) according to the equation $J = D_{SA} \times D_w \times \frac{dC}{dz}$. Thus the 15% variation in the D_{SA} (Fig. 3.6) will lead to 15% variation in the flux.

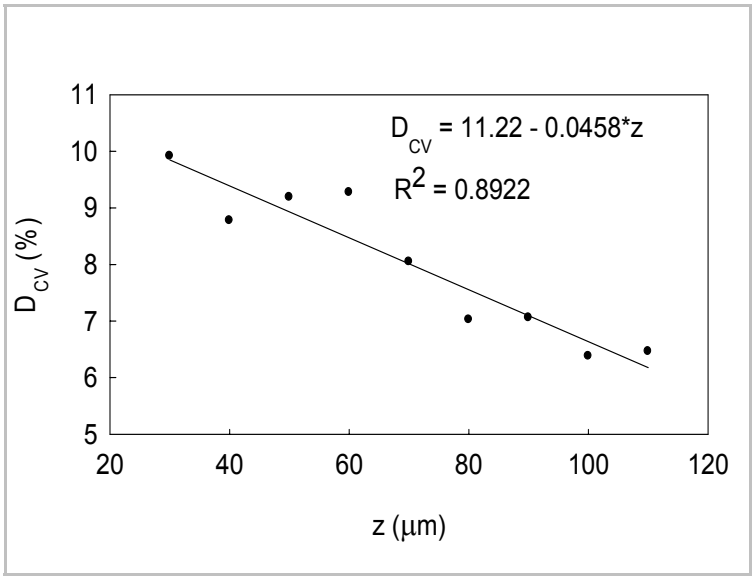

Fig. 3.7. The coefficient of variation in surface averaged effective diffusivity (D_{CV}) plotted against the distance from the bottom (z) of the biofilm.

Fig. 3.8 shows the variation in D_{SA} inside the biofilm. Two curves were fitted to describe the relations between D_{SA} and distance: a linear relation and a nonlinear, exponential relation.

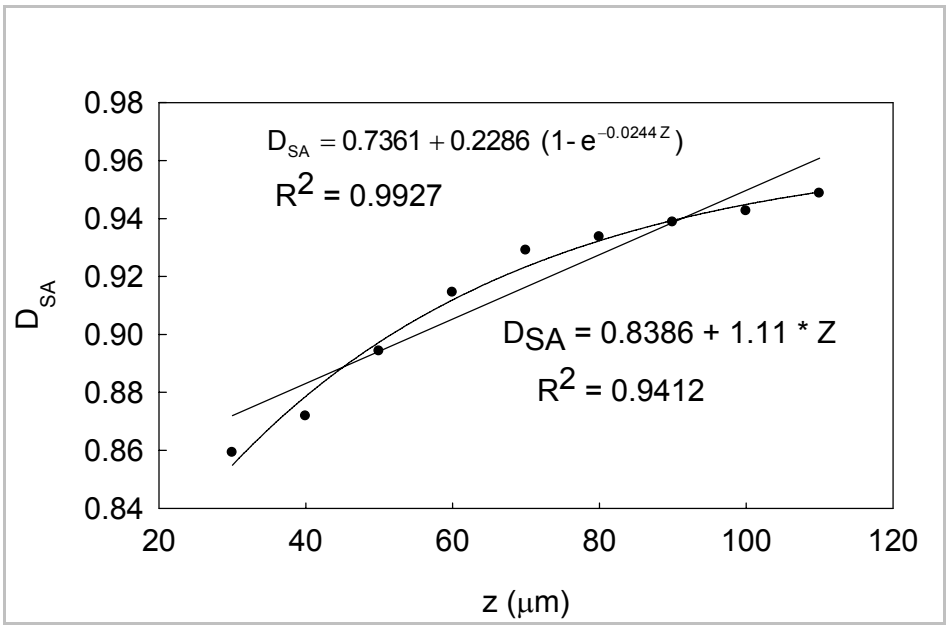

Fig. 3.8. Variation in surface averaged relative effective diffusivity with distance from the bottom of the biofilm (relative effective diffusivity variation inside the biofilm).

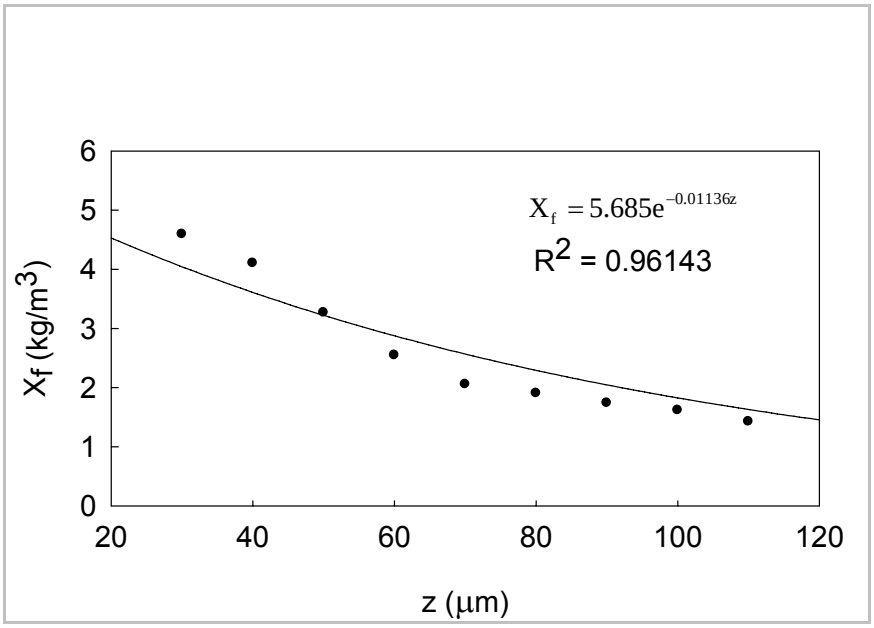

Fig. 3.9. Variation of biofilm density inside the biofilm.

The nonlinear relation shows a better fit, has a higher regression coefficient, and is clearly the preferred relation. However, the difference between the linear and nonlinear fits is not dramatic. Beyenal and Lewandowski (2001) in the model of stratified biofilms assume that this relation is linear. From the results in this work, it appears that a nonlinear relation would be beneficial.

The data below 30 μm were not included in the correlation plots because the local diffusivity microelectrode readings are not accurate that close to the bottom of the biofilm, as explained by Beyenal and Lewandowski (2001).

The correlations between the relative effective diffusivity and other parameters (areal porosity and dissolved oxygen concentration) are easier to interpret if relative effective diffusivity is converted into equivalent density of the biofilm using Eqn. 1.1. (Fig. 3.9). As expected, biofilm density increases towards the bottom of the biofilm (Fig. 3.9), which is in agreement with the fact that the relative effective diffusivity decreases towards the bottom of the biofilm.

As shown in Fig. 3.7, the coefficient of variation of relative effective diffusivity increases linearly towards the bottom of the biofilm. This effect may be caused by (1) a decrease in biofilm porosity near the bottom, (2) the increase in the biomass density in microcolonies near the bottom, or (3) both. Fig. 3.11 shows that the biofilm porosity near the bottom does not change much. Consequently, the main factor causing the increase in diffusivity near the bottom is the increase in the density of microcolonies. Fig. 3.10 shows the surface plots of the local relative effective diffusivities for different distances from the bottom of

the biofilm. The local effective diffusivities are almost constant above the biofilm and show increased variability as the bottom of the biofilm is approached.

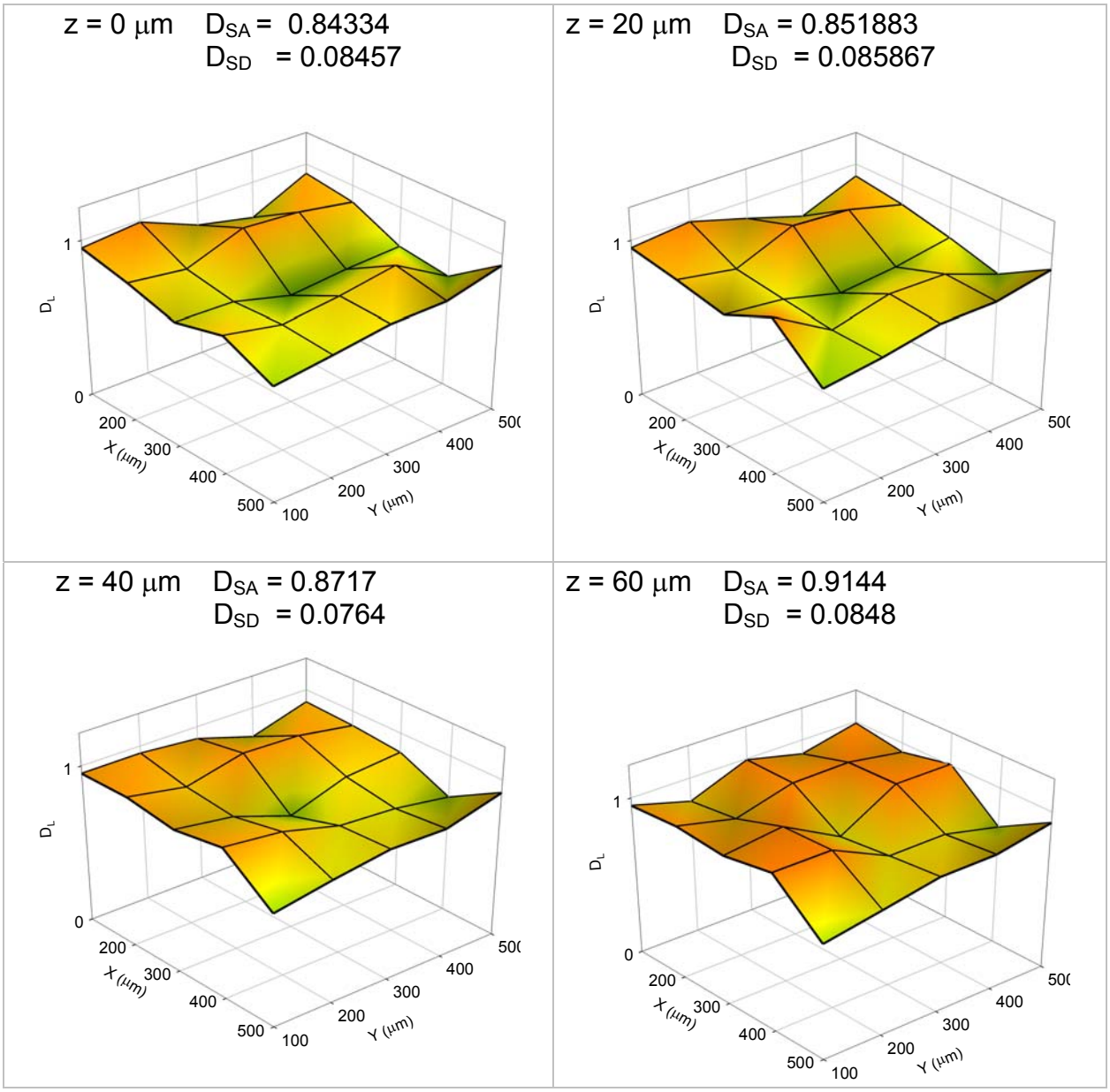

z = 80 μm D_{SA} = 0.9335
D_{SD} = 0.0655

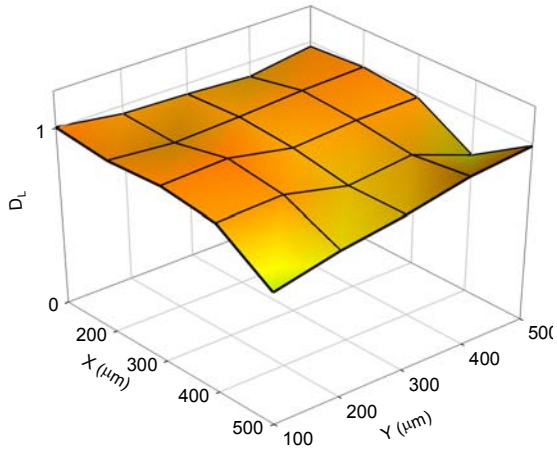

z = 100 μm D_{SA} = 0.9425
D_{SD} = 0.0601

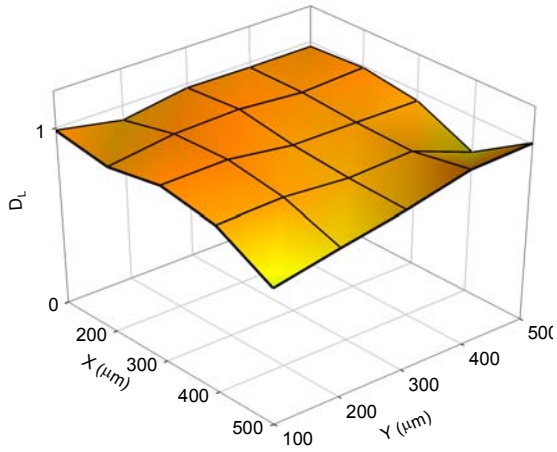

z = 120 μm D_{SA} = 0.9501
D_{SD} = 0.0625

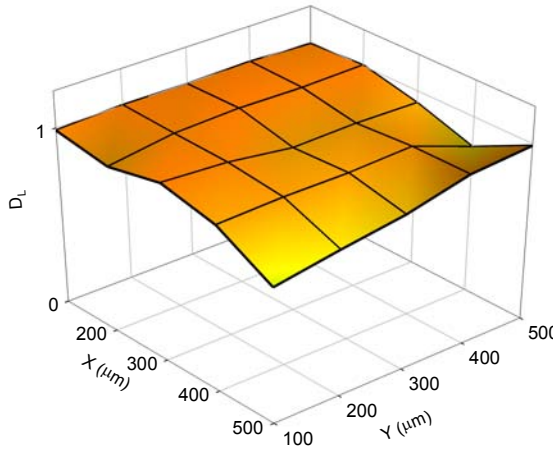

z = 140 μm D_{SA} = 0.9558
D_{SD} = 0.0533

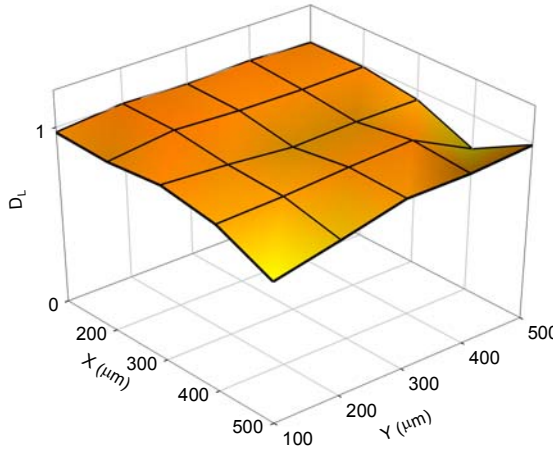

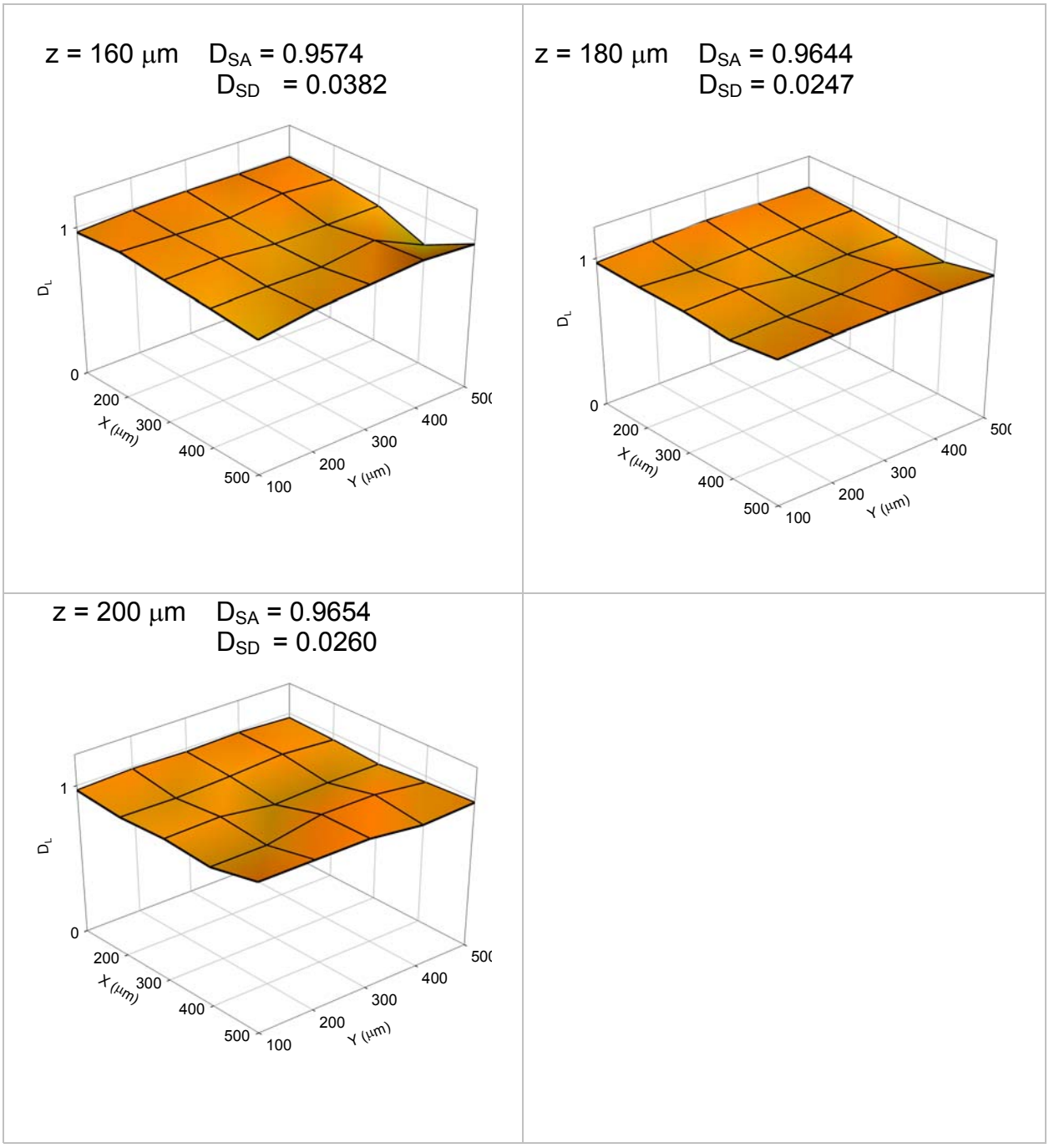

Fig. 3.10. The local relative effective diffusivities at different layers of the biofilm. Where: D_{SA} is the surface averaged relative effective diffusivity and D_{SD} is the standard deviation of the local relative effective diffusivity. z = 0 represents the bottom of the biofilm.

Areal Porosity of the Biofilm

Fig. 3.11shows that the areal porosity in the biofilm decreases toward the bottom of the biofilm and that it is almost constant between 0 and 70 μm from the bottom. The standard deviation (shown as the error bars) increases towards the bottom. However, below 70 μm from the bottom, the standard deviation does not change significantly. Similarly, the coefficient of variation is the lowest near the surface of the biofilm and it does not change significantly inside the biofilm (Fig. 3.11). It is important to note that even though the areal porosity is constant below 70 μm, the density of the biofilm below 70 μm still decreases toward the bottom of the biofilm (Fig. 3.9).

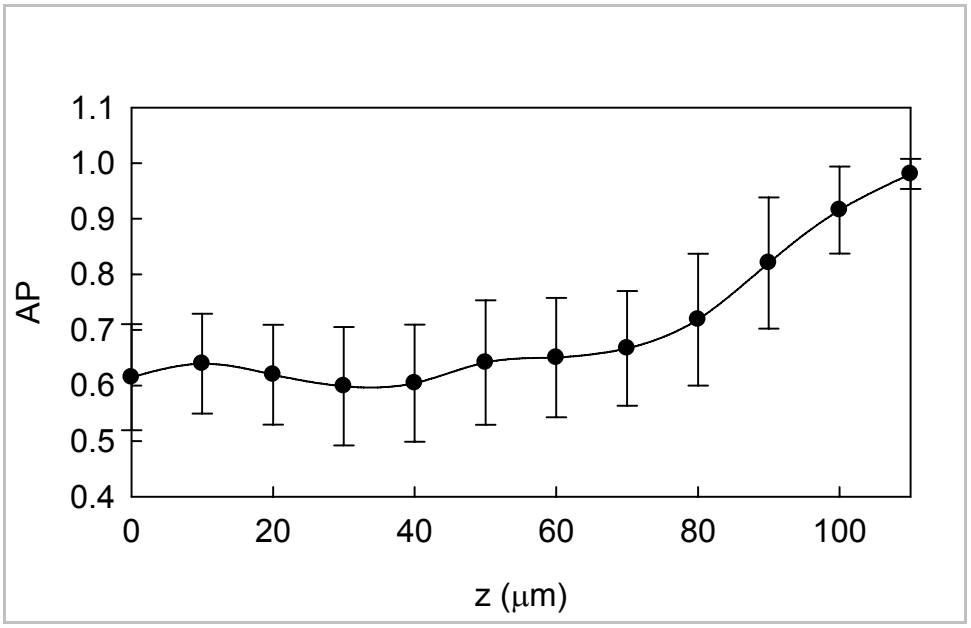

Fig. 3.11. Areal porosity vs. distance from the bottom of the biofilm. On average, the areal porosity decreases towards the bottom of the biofilm. However, it remains almost constant near the bottom (z=0).

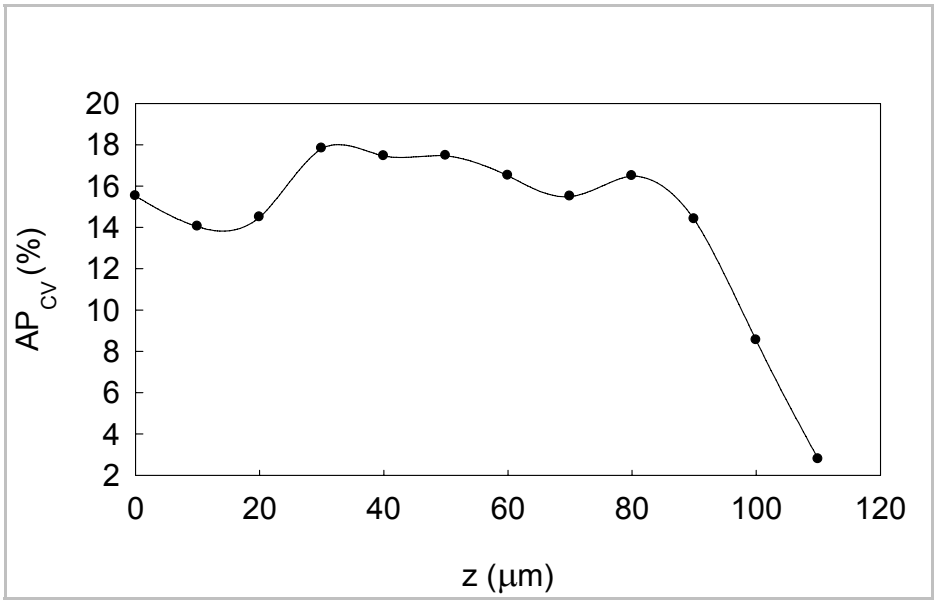

Fig. 3.12. The coefficient of variation of areal porosity (AP_{CV}) plotted against the distance from the bottom of the biofilm.

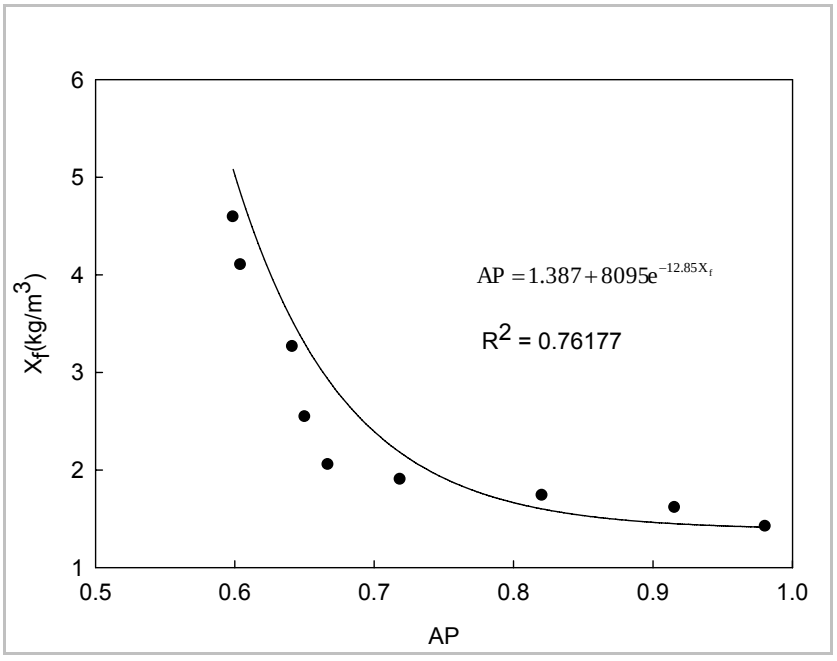

Fig. 3.13. Variation of biofilm density with areal porosity.

Fig. 3.13 shows that the density of the biofilm increases with decreasing areal porosity, i.e., a lower biomass coverage (high AP) results in a lower biomass density and a higher biomass coverage (low AP) results in a higher biomass density.

Correlation of D_{SA} with AP and C_{SA}

Surface averaged relative effective diffusivity is strongly correlated with areal porosity (Fig. 3.14). Diffusivity is affected by the biomass density and by the areal porosity.

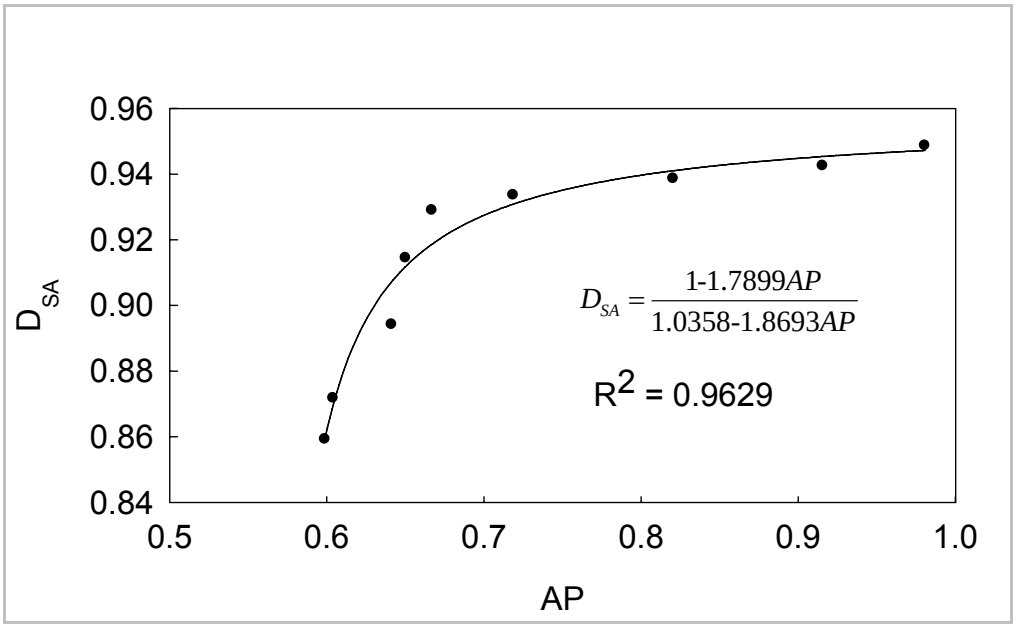

Fig. 3.14. Variation of surface averaged relative effective diffusivity with areal porosity. The two parameters are measured at the same distance from the bottom.

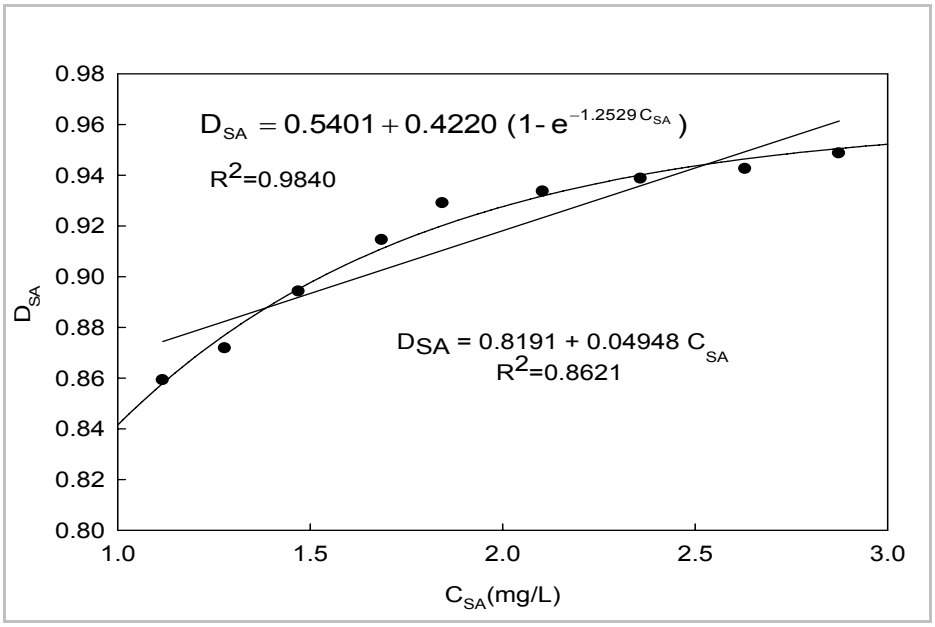

Fig. 3.15. Surface averaged relative effective diffusivity (D_{SA}) vs. surface averaged dissolved oxygen concentration (C_{SA}). The two parameters were measured at the same distance from the bottom.

The data in Fig. 3.15 show that the surface averaged relative effective diffusivity increases with increasing dissolved oxygen concentration. A higher relative effective diffusivity results in faster diffusion of the nutrient and a lower diffusivity results in slower diffusion of the nutrient. Since relative effective diffusivity is high at the top of the biofilm, the nutrient from the bulk diffuses quickly to the upper layers of the biofilm: hence the observed higher concentrations in the upper layers of the biofilm. Since the lower layers of the biofilm have smaller values for relative effective diffusivity, the diffusion of the nutrient to the lower layers is slower, resulting in lower concentrations in the lower layers of the biofilm. Measurement results which demonstrate correlations among other parameters are presented in Appendix 1.

Summary

The working hypothesis of this research was equivalent to the main assumption of the conceptual model of stratified biofilms, that the measured parameters within the space occupied by the biofilm are related when quantified as average values in layers of the biofilm, but that these relations are not necessarily obvious when analyzing the data of individual measurements. The results of this study demonstrate that this hypothesis is correct: the measured parameters—surface averaged effective diffusivity, surface averaged areal porosity, and surface averaged oxygen—correlate with each other significantly. The most spectacular demonstration that individual results, not averaged over the surface area, do not behave in a predictable fashion is measurement of the effective diffusivity profile (Fig. 3.5). The same results, when averaged as recommended by the model of stratified biofilms, exhibit a clearly visible trend (Fig. 3.6).

In the course of this study, the heterogeneity of any parameter measured in the space occupied by the biofilm was defined as the measure of the nonuniform distribution of that parameter in the biofilm. To quantify the heterogeneity of measured parameters, we typically use standard deviations measured within single layers of the biofilm. In this study, the distribution of the data was evaluated using the standard deviation and using the coefficient of variation. The results show that the standard deviation remains a reliable descriptor of heterogeneity in individual layers of biofilm. However, the results

also demonstrate that when all layers are compared, the coefficient of variation is a more descriptive parameter of heterogeneity than the standard deviation. Standard deviations are, by definition, average deviations from the average, and, as such, their numerical values are affected by the numerical values of the averages. This effect is not relevant when only one set of data is considered, but when the standard deviation is considered as a descriptor of heterogeneity, the values of the standard deviations should be normalized. Therefore, we consider the coefficient of variation, which carries the same information as the standard deviation but is numerically normalized with respect to the average, a more reliable descriptor of heterogeneity that the standard deviation.

Conclusions

The goals of this study were to (1) correlate the dissolved oxygen concentration in a biofilm with relative effective diffusivity, (2) correlate the dissolved oxygen concentration in the biofilm with areal porosity, and (3) correlate the relative effective diffusivity with the areal porosity. We used the conceptual model of stratified biofilms to interpret the results of the measurements. As a result of the measurements presented above, we conclude that in biofilms of *Pseudomonas aeruginosa* PAO1 we can present meaningful correlations among the 3-D distributions of various parameters in the biofilm. Specifically, we have demonstrated that:

1. Local concentrations of dissolved oxygen and local relative effective diffusivities do not correlate with each other or with the areal porosity.
2. Surface averaged dissolved oxygen concentration, surface averaged relative effective diffusivity, and areal porosity decrease towards the bottom of the biofilm.
3. Surface averaged dissolved oxygen concentration and surface averaged relative effective diffusivity correlate with each other and with areal porosity.
4. The coefficient of variation of the surface averaged dissolved oxygen concentration and the surface averaged relative effective diffusivity increases towards the bottom.

REFERENCES CITED

Atkinson, B. And I. J. Davies. "Overall Rate Of Substrate Uptake (Reaction) By Microbial Films .1. Biological Rate Equation." Transactions Of The Institution Of Chemical Engineers 52.3 (1974): 248-59.

Beyenal, H. Et Al. "Three-Dimensional Biofilm Structure Quantification." Journal Of Microbiological Methods 59.3 (2004): 395-413.

Beyenal, H. And Z. Lewandowski. "Internal And External Mass Transfer In Biofilms Grown At Various Flow Velocities." Biotechnology Progress 18.1 (2002): 55-61.

Beyenal, H. And Z. Lewandowski. "Modeling Mass Transport And Microbial Activity In Stratified Biofilms." Chemical Engineering Science 60.15 (2005): 4337-48.

Beyenal, H., Z. Lewandowski, And G. Harkin. "Quantifying Biofilm Structure: Facts And Fiction." Biofouling 20.1 (2004): 1-23.

Beyenal, H., A. Tanyolac, And Z. Lewandowski. "Measurement Of Local Effective Diffusivity In Heterogeneous Biofilms." Water Science And Technology 38.8-9 (1998): 171-78.

Bishop, P. L. "Biofilm Structure And Kinetics." Water Science And Technology 36.1 (1997): 287-94.

Debeer, D., P. Stoodley, And Z. Lewandowski. "Liquid Flow In Heterogeneous Biofilms." Biotechnology And Bioengineering 44.5 (1994): 636-41.

Debeer, D., P. Stoodley, And Z. Lewandowski. "Liquid Flow And Mass Transport In Heterogeneous Biofilms." Water Research 30.11 (1996): 2761-65.

Debeer, D., P. Stoodley, And Z. Lewandowski. "Measurement Of Local Diffusion Coefficients In Biofilms By Microinjection And Confocal Microscopy." Biotechnology And Bioengineering 53.2 (1997): 151-58.

Debeer, D. Et Al. "Effects Of Biofilm Structures On Oxygen Distribution And Mass-Transport." Biotechnology And Bioengineering 43.11 (1994): 1131-38.

Hermanowicz, S. W. "A Simple 2d Biofilm Model Yields A Variety Of Morphological Features." Mathematical Biosciences 169.1 (2001): 1-14.

Kreft, J. U. Et Al. "Individual-Based Modelling Of Biofilms." Microbiology-Sgm 147 (2001): 2897-912.

Morgenroth, E., M. C. M. Van Loosdrecht, And O. Wanner. "Biofilm Models For The Practitioner." Water Science And Technology 41.4-5 (2000): 509-12.

Noguera, D. R., S. Okabe, And C. Picioreanu. "Biofilm Modeling: Present Status And Future Directions." Water Science And Technology 39.7 (1999): 273-78.

Picioreanu, C., M. C. M. Van Loosdrecht, And J. J. Heijnen. "A New Combined Differential-Discrete Cellular Automaton Approach For Biofilm Modeling: Application For Growth In Gel Beads." Biotechnology And Bioengineering 57.6 (1998): 718-31.

Picioreanu, C., M. C. M. Van Loosdrecht, And J. J. Heijnen. "Mathematical Modeling Of Biofilm Structure With A Hybrid Differential-Discrete Cellular Automaton Approach." Biotechnology And Bioengineering 58.1 (1998): 101-16.

Picioreanu, C., M. C. M. Van Loosdrecht, And J. J. Heijnen. "A Theoretical Study On The Effect Of Surface Roughness On Mass Transport And Transformation In Biofilms." Biotechnology And Bioengineering 68.4 (2000): 355-69.

Picioreanu, C., M. C. M. Van Loosdrecht, And J. J. Heijnen. "Effect Of Diffusive And Convective Substrate Transport On Biofilm Structure Formation: A Two-Dimensional Modeling Study." Biotechnology And Bioengineering 69.5 (2000): 504-15.

Picioreanu, C., M. C. M. Van Loosdrecht, And J. J. Heijnen. "Two-Dimensional Model Of Biofilm Detachment Caused By Internal Stress From Liquid Flow." Biotechnology And Bioengineering 72.2 (2001): 205-18.

Pizarro, G., D. Griffeath, And D. R. Noguera. "Quantitative Cellular Automaton Model For Biofilms." Journal Of Environmental Engineering-Asce 127.9 (2001): 782-89.

Rasmussen, K. And Z. Lewandowski. "Microelectrode Measurements Of Local Mass Transport Rates In Heterogeneous Biofilms." Biotechnology And Bioengineering 59.3 (1998): 302-09.

Rittmann, B. E. And C. W. Brunner. "The Nonsteady-State-Biofilm Process For Advanced Organics Removal." Journal Water Pollution Control Federation 56.7 (1984): 874-80.

Rittmann, B. E. And K. Dovantzis. "Dual Limitation Of Biofilm Kinetics." Water Research 17.12 (1983): 1727-34.

Rittmann, B. E. And P. L Mccarty. "Evaluation Of Steady-State-Biofilm Kinetics." Biotechnology And Bioengineering 22.11 (1980): 2359-73.

Rittmann, B. E. And P. L Mccarty. "Model Of Steady-State-Biofilm Kinetics." Biotechnology And Bioengineering 22.11 (1980): 2343-57.

Soda, S., E. Heinzle, And M. Fujita. "Modeling And Simulation Of Competition Between Two Microorganisms For A Single Inhibitory Substrate In A Biofilm Reactor." Biotechnology And Bioengineering 66.4 (1999): 258-64.

Stewart, P. S. Et Al. "Modeling Biocide Action Against Biofilms." Biotechnology And Bioengineering 49.4 (1996): 445-55.

Stoodley, P. Et Al. "Relationship Between Mass Transfer Coefficient And Liquid Flow Velocity In Heterogenous Biofilms Using Microelectrodes And Confocal Microscopy." Biotechnology And Bioengineering 56.6 (1997): 681-88.

Suidan, M. T. Et Al. "Optimization Modeling Of Anaerobic Biofilm Reactors." Water Science And Technology 30.12 (1994): 347-55.

Sun, A. K., J. Hong, And T. K. Wood. "Modeling Trichloroethylene Degradation By A Recombinant Pseudomonad Expressing Toluene Ortho-Monooxygenase In A Fixed-Film Bioreactor." Biotechnology And Bioengineering 59.1 (1998): 40-51.

Wanner, O., A. B. Cunningham, And R. Lundman. "Modeling Biofilm Accumulation And Mass-Transport In A Porous-Medium Under High Substrate Loading." Biotechnology And Bioengineering 47.6 (1995): 703-12.

Wanner, O. And W. Gujer. "A Multispecies Biofilm Model." Biotechnology And Bioengineering 28.3 (1986): 314-28.

Wanner, O. And P. Reichert. "Mathematical Modeling Of Mixed-Culture Biofilms." Biotechnology And Bioengineering 49.2 (1996): 172-84.

Wanner, O. And P. Reichert. "Mathematical Modeling Of Mixed-Culture Biofilms." Biotechnology And Bioengineering 49.2 (1996): 172-84.

Williamson, K. And P. L Mccarty. "Verification Studies Of Biofilm Model For Bacterial Substrate Utilization." Journal Water Pollution Control Federation 48.2 (1976): 281-96.

Wimpenny, J., W. Manz, And U. Szewzyk. "Heterogeneity In Biofilms." Fems Microbiology Reviews 24.5 (2000): 661-71.

Wimpenny, J. W. T. And R. Colasanti. "A More Unifying Hypothesis For Biofilm Structures - A Reply." Fems Microbiology Ecology 24.2 (1997): 185-86.

Wimpenny, J. W. T. And R. Colasanti. "A Unifying Hypothesis For The Structure Of Microbial Biofilms Based On Cellular Automaton Models." Fems Microbiology Ecology 22.1 (1997): 1-16.

Yang, S. N. And Z. Lewandowski. "Measurement Of Local Mass-Transfer Coefficient In Biofilms." Biotechnology And Bioengineering 48.6 (1995): 737-44.

Revsbech. N.P And Jorgensen. B.B "Microelectrodes - Their Use In Microbial Ecology." Advances In Microbial Ecology
9 (1986) 293-352

Hunt. S.M, Hamilton. M.A, Sears. J.T, Harkin. G And Reno. J. "A Computer Investigation Of Chemically Mediated Detachment In Bacterial Biofilms". Microbiology-Sgm 149.5 (2003) 1155-1163.5

APPENDIX A

OTHER SELECTED CORRELATIONS

In this appendix, measurement results which demonstrate correlations among other parameters are presented.

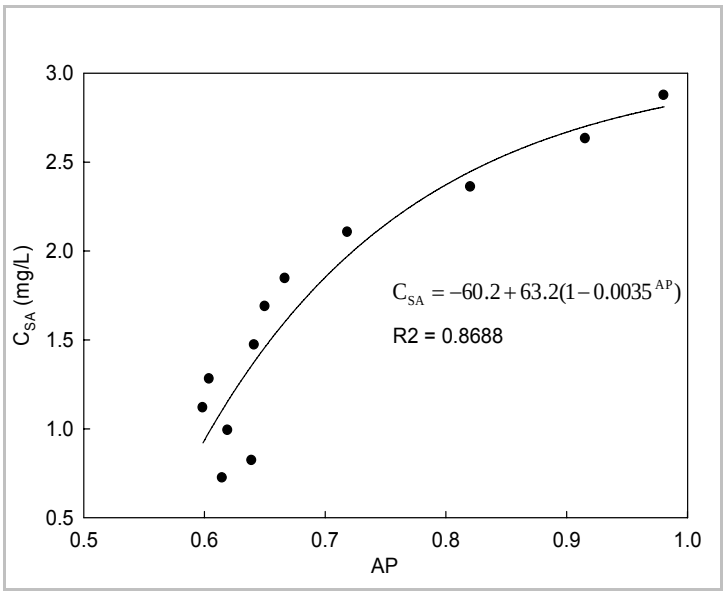

Fig. 4.1. Surface averaged dissolved oxygen concentration versus areal porosity. The two parameters were measured at the same distance from the bottom of the biofilm.

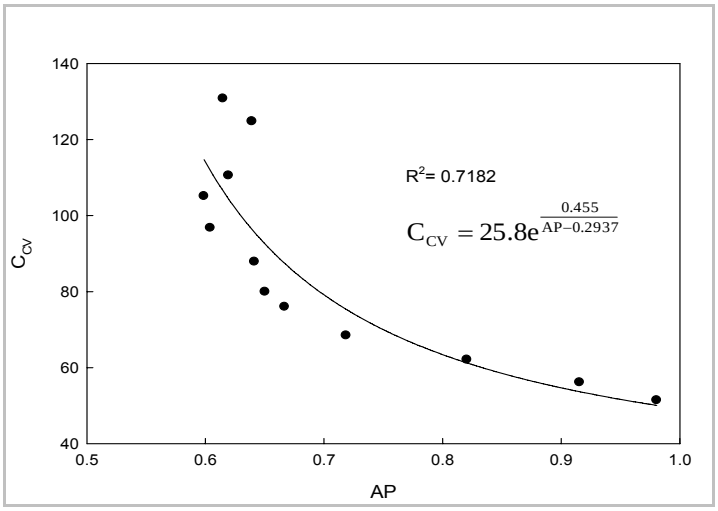

Fig. 4.2. Plot of the coefficient of variation in the dissolved oxygen concentration vs. areal porosity. The two parameters were measured at the same distance from the bottom of the biofilm.

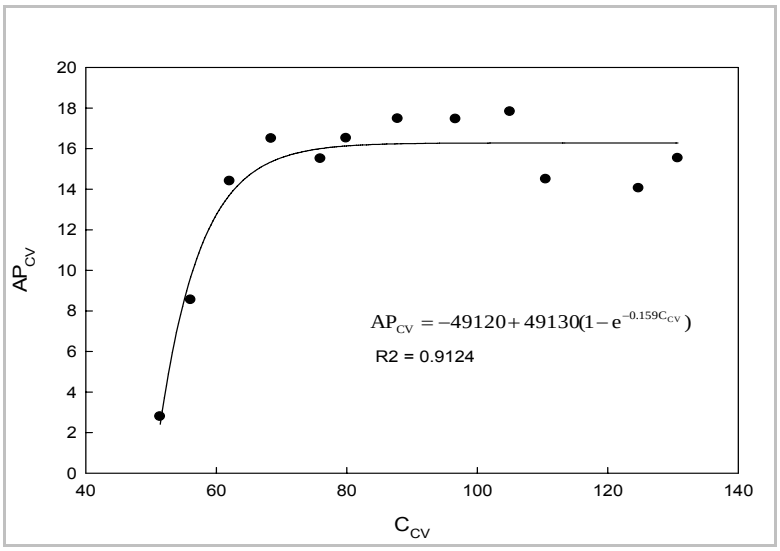

Fig. 4.3. Variation of the standard deviation of surface averaged dissolved oxygen concentration with the coefficient of variation of areal porosity. The two parameters were measured at the same distance from the bottom.

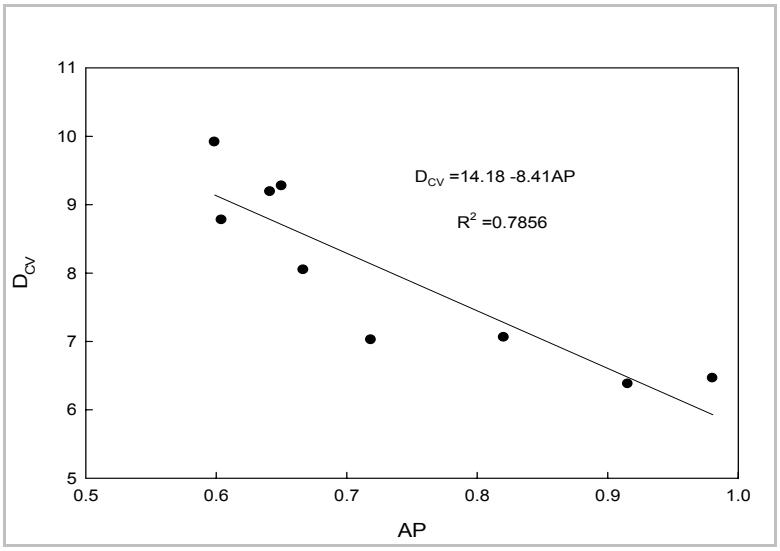

Fig. 4.4. The correlation between the coefficient of the variation of surface averaged relative effective diffusivity (D_{CV}) and the areal porosity. The two parameters were measured at the same distance from the bottom.

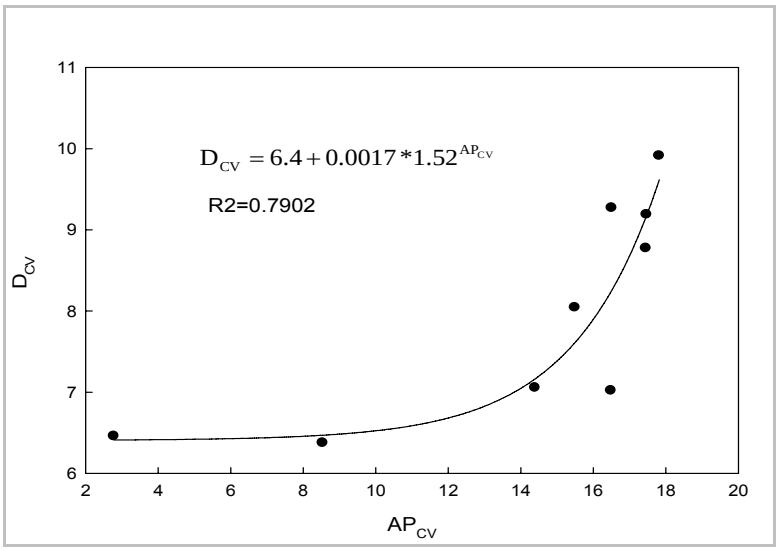

Fig. 4.5. Coefficient of variation of surface averaged relative effective diffusivity (D_{CV}) vs. coefficient of variation of areal porosity. The two parameters were measured at the same distance from the bottom.

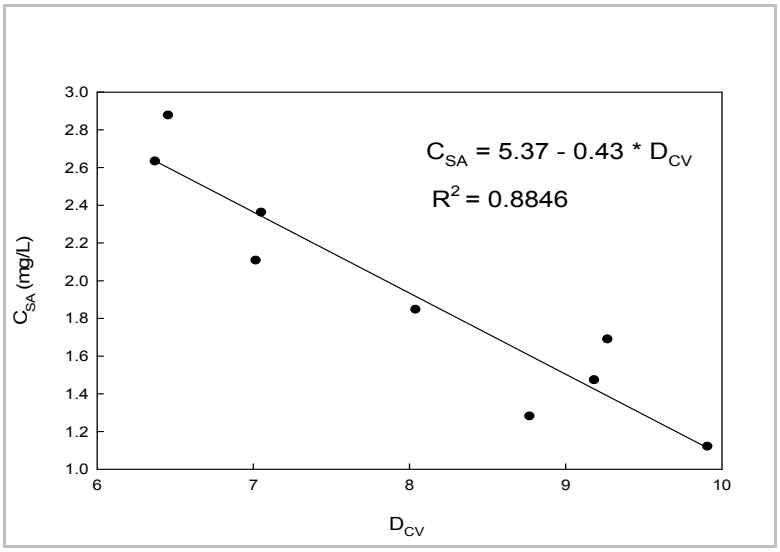

Fig. 4.6. Correlation between surface averaged dissolved oxygen concentration (C_{SA}) and the coefficient of variation of surface averaged relative effective diffusivity (D_{CV}). The two parameters were measured at the same distance from the bottom.

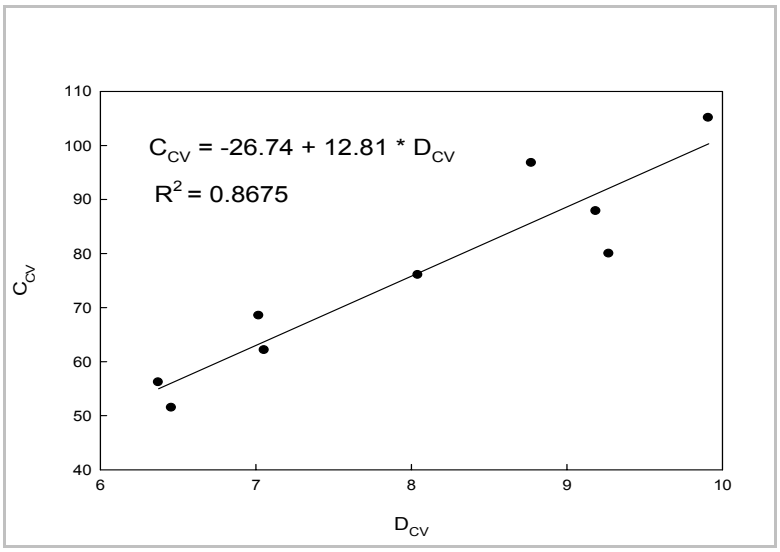

Fig. 4.7. Correlation between the coefficient of variation of surface averaged dissolved oxygen concentration (C_{CV}) and the coefficient of variation of surface averaged relative effective diffusivity (D_{CV}).

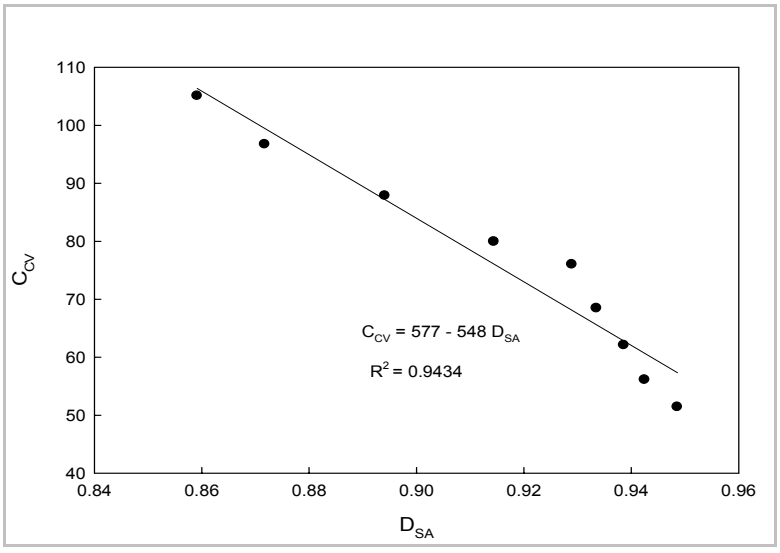

Fig. 4.8. Variation of coefficient of variation of surface averaged dissolved oxygen concentration with surface averaged relative effective diffusivity.